

January 2010

## Reaction of the C<sub>2</sub>H radical with 1-Butyne (C<sub>4</sub>H<sub>6</sub>): Low Temperature Kinetics and Isomer-Specific Product Detection

Satchin Soorkia

Adam J. Trevitt  
*University of Wollongong*, [adamt@uow.edu.au](mailto:adamt@uow.edu.au)


Talitha M. Selby

David L. Osborn

Craig A. Taatjes

*See next page for additional authors*

Follow this and additional works at: <https://ro.uow.edu.au/scipapers>

 Part of the [Life Sciences Commons](#), [Physical Sciences and Mathematics Commons](#), and the [Social and Behavioral Sciences Commons](#)

---

### Recommended Citation

Soorkia, Satchin; Trevitt, Adam J.; Selby, Talitha M.; Osborn, David L.; Taatjes, Craig A.; Wilson, Kevin R.; and Leone, Stephen R.: Reaction of the C<sub>2</sub>H radical with 1-Butyne (C<sub>4</sub>H<sub>6</sub>): Low Temperature Kinetics and Isomer-Specific Product Detection 2010, 3340-3354.  
<https://ro.uow.edu.au/scipapers/474>

Research Online is the open access institutional repository for the University of Wollongong. For further information contact the UOW Library: [research-pubs@uow.edu.au](mailto:research-pubs@uow.edu.au)

---

## Reaction of the C<sub>2</sub>H radical with 1-Butyne (C<sub>4</sub>H<sub>6</sub>): Low Temperature Kinetics and Isomer-Specific Product Detection

### Keywords

butyne, c<sub>4</sub>h<sub>6</sub>, reaction, low, radical, 1, temperature, kinetics, isomer, specific, product, detection, c<sub>2</sub>h, GeoQUEST

### Disciplines

Life Sciences | Physical Sciences and Mathematics | Social and Behavioral Sciences

### Publication Details

Soorkia, S., Trevitt, A. J., Selby, T. M., Osborn, D. L., Taatjes, C. A., Wilson, K. R. & Leone, S. R. (2010). Reaction of the C<sub>2</sub>H radical with 1-Butyne (C<sub>4</sub>H<sub>6</sub>): Low Temperature Kinetics and Isomer-Specific Product Detection. *The Journal of Physical Chemistry Part A: Molecules, Spectroscopy, Kinetics, Environment and General Theory*, 114 (9), 3340-3354.

### Authors

Satchin Soorkia, Adam J. Trevitt, Talitha M. Selby, David L. Osborn, Craig A. Taatjes, Kevin R. Wilson, and Stephen R. Leone

# Reaction of the C<sub>2</sub>H Radical with 1-Butyne (C<sub>4</sub>H<sub>6</sub>): Low-Temperature Kinetics and Isomer-Specific Product Detection<sup>†</sup>

**Satchin Soorkia**

*Departments of Chemistry and Physics, University of California, Berkeley, California 94720*

**Adam J. Trevitt**

*School of Chemistry, University of Wollongong, Wollongong, New South Wales 2522, Australia*

**Talitha M. Selby**

*Department of Chemistry, University of Wisconsin—Washington County, West Bend, Wisconsin 53095*

**David L. Osborn and Craig A. Taatjes**

*Combustion Research Facility, Mail Stop 9055, Sandia National Laboratories, Livermore, California 94551-0969*

**Kevin R. Wilson**

*Chemical Sciences Division, Lawrence Berkeley National Laboratory, 1 Cyclotron Road, Berkeley, California 94720*

**Stephen R. Leone\***

*Departments of Chemistry and Physics, University of California, Berkeley, California 94720 and Chemical Sciences Division, Lawrence Berkeley National Laboratory, 1 Cyclotron Road, Berkeley, California 94720*

*Received: November 23, 2009; Revised Manuscript Received: December 26, 2009*

The rate coefficient for the reaction of the ethynyl radical (C<sub>2</sub>H) with 1-butyne (H–C≡C–CH<sub>2</sub>–CH<sub>3</sub>) is measured in a pulsed Laval nozzle apparatus. Ethynyl radicals are formed by laser photolysis of acetylene (C<sub>2</sub>H<sub>2</sub>) at 193 nm and detected via chemiluminescence (C<sub>2</sub>H + O<sub>2</sub> → CH (A<sup>2</sup>Δ) + CO<sub>2</sub>). The rate coefficients are measured over the temperature range of 74–295 K. The C<sub>2</sub>H + 1-butyne reaction exhibits no barrier and occurs with rate constants close to the collision limit. The temperature-dependent rate coefficients can be fit within experimental uncertainties by the expression  $k = (2.4 \pm 0.5) \times 10^{-10} (T/295 \text{ K})^{-(0.04 \pm 0.03)} \text{ cm}^3 \text{ molecule}^{-1} \text{ s}^{-1}$ . Reaction products are detected at room temperature (295 K) and 533 Pa using a multiplexed photoionization mass spectrometer (MPIMS) coupled to the tunable vacuum ultraviolet synchrotron radiation from the Advanced Light Source at the Lawrence Berkeley National Laboratory. Two product channels are identified for this reaction:  $m/z = 64$  (C<sub>5</sub>H<sub>4</sub>) and  $m/z = 78$  (C<sub>6</sub>H<sub>6</sub>) corresponding to the CH<sub>3</sub>-loss and H-loss channels, respectively. Photoionization efficiency (PIE) curves are used to analyze the isomeric composition of both product channels. The C<sub>5</sub>H<sub>4</sub> products are found to be exclusively linear isomers composed of ethynylallene and methylidyneacetylene in a 4:1 ratio. In contrast, the C<sub>6</sub>H<sub>6</sub> product channel includes two cyclic isomers, fulvene 18(±5)% and 3,4-dimethylenecyclobut-1-ene (DMCB) 32(±8)%, as well as three linear isomers, 2-ethynyl-1,3-butadiene 8(±5)%, 3,4-hexadiene-1-yne 28(±8)%, and 1,3-hexadiyne 14(±5)%. Within experimental uncertainties, we do not see appreciable amounts of benzene and an upper limit of 10% is estimated. Diacetylene (C<sub>4</sub>H<sub>2</sub>) formation via the C<sub>2</sub>H<sub>5</sub>-loss channel is also thermodynamically possible but cannot be observed due to experimental limitations. The implications of these results for modeling of planetary atmospheres, especially of Saturn's largest moon Titan and the relationships to combustion reactions, are discussed.

## 1. Introduction

The ethynyl radical, C<sub>2</sub>H, is an important polyatomic radical in the interstellar medium.<sup>1</sup> Its relative abundance is a marker of the carbon richness of its environment, as observed on Saturn's largest moon, Titan. C<sub>2</sub>H radicals are formed in the cold, dense, structured, and complex atmosphere of Titan<sup>2–4</sup> by

the photolysis (via solar radiation) of acetylene.<sup>5</sup> Moreover, ethynyl radicals are believed to play a major role in the molecular weight growth of larger carbonaceous species. In a model proposed by Wilson and Atreya,<sup>6</sup> to account for the dense haze observed on Titan, the reaction of the C<sub>2</sub>H radical with acetylene is a key step in the formation of longer chain polyynic molecules (e.g., C<sub>4</sub>H<sub>2</sub> and C<sub>6</sub>H<sub>2</sub>). These polyynes can subsequently react further with C<sub>2</sub>H radicals to eventually form much larger polymeric species that ultimately contribute to the

<sup>†</sup> Part of the "Benoît Soep Festschrift".

\* Corresponding author, srl@berkeley.edu. On appointment as a Miller Research Professor in the Miller Institute for Basic Research in Science.

observed photochemically active and colored organic haze.<sup>7</sup> Similarly, C<sub>2</sub>H is a key radical in the formation of polycyclic aromatic hydrocarbons (PAHs),<sup>6</sup> which are believed to play an important role in interstellar chemistry.<sup>8,9</sup>

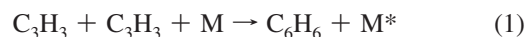
Benzene (C<sub>6</sub>H<sub>6</sub>), the simplest aromatic hydrocarbon, is considered to be a precursor for larger PAH formation and its recent identification on Titan<sup>10</sup> strongly suggests that much more complex PAH synthesis may proceed in the cold atmosphere of the Saturnian moon. Recently, Mebel and co-workers<sup>11</sup> proposed a novel ethynyl addition mechanism (EAM) as a viable alternative to the high-temperature hydrogen abstraction–C<sub>2</sub>H<sub>2</sub> addition (HACA)<sup>12</sup> mechanism for the formation of PAHs at very low temperatures. As described,<sup>11</sup> this mechanism is initiated by the addition of a C<sub>2</sub>H radical to an ortho-carbon of ethynylbenzene (C<sub>6</sub>H<sub>5</sub>–C≡C–H), and the reactive intermediate subsequently loses a H atom to form 1,2-diethynylbenzene. The latter then reacts with a second C<sub>2</sub>H radical via addition to one of the carbon atoms on the ethynyl side chains. Ring closure of the intermediate leads to the formation of the ethynyl-substituted bicyclic naphthalene core. The authors conclude that since the stepwise addition of C<sub>2</sub>H radicals (followed by H atom elimination) to benzene, ethynylbenzene and 1,2-diethynylbenzene occurs without a barrier and with high exothermicity, the reactions of C<sub>2</sub>H radicals should be very fast, and they suggest that the reactions should proceed with rate constants on the order of 10<sup>-10</sup> cm<sup>3</sup> molecule<sup>-1</sup> s<sup>-1</sup> even at very low temperatures.

Since C<sub>2</sub>H is a key species in carbon-rich environments, it has been the subject of a number of studies.<sup>11,13–26</sup> In order to analyze and account for the presence of hydrocarbon species, modeling studies are of central importance in understanding the complex nature of Titan's atmosphere. Detailed models have been developed over the last few decades.<sup>6,27,28</sup> Low-temperature rate constants and product branching ratios are used when available to describe accurately and reliably<sup>29</sup> the chemical schemes<sup>27</sup> that are proposed. In this respect, much progress<sup>30</sup> has been made experimentally to obtain kinetic data on key chemical reactions down to very low temperatures relevant to interstellar chemistry. The CRESU (Cinétique de Réaction Chimique en Ecoulement Supersonique Uniforme) technique, pioneered by Rowe and co-workers,<sup>31,32</sup> involves the expansion of a gas mixture through a Laval nozzle and allows kinetic studies down to 10 K to examine chemistry under true interstellar conditions.<sup>31–35</sup> M. A. Smith and co-workers<sup>36,37</sup> developed a pulsed Laval apparatus that was adopted by Leone and co-workers<sup>21</sup> and Abel and co-workers.<sup>30</sup> The collimated supersonic flow generated by a Laval nozzle can be compared to a “wall-less flow tube reactor” in which reactions involving species with very low vapor pressures, that otherwise would tend to condense, can be studied. Moreover, the pulsed nozzle produces much less gas flow, requiring lower pumping speeds while yielding rate coefficients that are in satisfactory agreement with continuous flow measurements, as demonstrated in a collaborative work between Leone and co-workers and I. W. M. Smith and co-workers.<sup>13,25</sup>

Although numerous low-temperature kinetic measurements of the C<sub>2</sub>H radical with C<sub>2</sub> (in this paper, C<sub>n</sub> denotes a hydrocarbon species containing *n* carbon atoms) and C<sub>3</sub> hydrocarbons<sup>30</sup> have been performed during the past decade as well as product branching studies,<sup>17</sup> there are, to our knowledge, only a few measurements of rate coefficients with molecules having longer carbon chain lengths (C<sub>4</sub> and higher).<sup>38,39</sup> As pointed out by Sims and co-workers,<sup>38</sup> highly unsaturated hydrocarbon species with four and more carbon atoms tend to be very unstable compounds because, for example, diacetylene polymer-

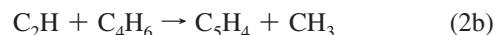
izes easily at room temperature. At the same time, the absence of these reactions in photochemical models can lead to underestimates of reaction pathways that otherwise would be non-negligible.<sup>40</sup> Furthermore, the photolysis of larger molecules may be a source of smaller neutral and radical species.<sup>40</sup> Therefore, it is suggested that future photochemical models will require including reactions of species containing four or more carbon atoms, hence taking into account the underlying contributions of higher molecular weight species for more accurate chemical descriptions of Titan's atmosphere in models.

A recent study by Vuitton and co-workers<sup>41</sup> provides insight into the formation and distribution of benzene, a C<sub>6</sub> hydrocarbon species, on Titan. The three-body propargyl recombination reaction (see eq 1) used in models<sup>42,43</sup> fails to predict the large mole fractions of benzene observed in the thermosphere on Titan.



Indeed, three-body reactions are unlikely at low densities (~10<sup>12</sup> cm<sup>-3</sup> of N<sub>2</sub> at an altitude of ~800 km).<sup>41</sup> Considering the time constants of key ion reactions,<sup>41</sup> the authors suggest that benzene in the ionosphere is likely produced by ion–molecule chemistry. The globally averaged column-integrated production rate of benzene in the ionosphere (~10<sup>7</sup> cm<sup>-2</sup> s<sup>-1</sup>) is found to be of the same order of magnitude as the radical–neutral production rate (~4 × 10<sup>6</sup> cm<sup>-2</sup> s<sup>-1</sup>). The radical–neutral (C<sub>2</sub>H + C<sub>4</sub>H<sub>6</sub>) and radical–radical (C<sub>2</sub>H<sub>3</sub> + C<sub>4</sub>H<sub>3</sub>) reactions are identified as potential reactions to be included in models, and the authors strongly emphasized that low-temperature rate coefficients and product identification are required for these reactions. Conversely, in a recent combustion study, Hansen and co-workers<sup>44</sup> showed that C<sub>6</sub>H<sub>6</sub> is formed primarily through C<sub>3</sub>H<sub>3</sub> + C<sub>3</sub>H<sub>3</sub> and *i*-C<sub>4</sub>H<sub>5</sub> + C<sub>2</sub>H<sub>2</sub>. In flames, the concentration of propargyl radicals is much higher and the formation of benzene via this pathway is more favorable. It is therefore of fundamental interest to explore the possible formation reactions of C<sub>6</sub> molecules in the cold, low pressure, and photochemically driven atmospheres of the outer planets, and especially Titan.

Carbon-containing radicals usually react with unsaturated hydrocarbon species where a short-lived intermediate<sup>45</sup> is formed and decomposes to give the substituted product, i.e., H-loss channel or CH<sub>3</sub>-loss channel<sup>17</sup> (see eqs 2a and 2b). The reaction of C<sub>2</sub>H with a C<sub>4</sub> substituted alkyne, 1-butyne (C<sub>4</sub>H<sub>6</sub>), is one such reaction with the possibility of forming cyclic C<sub>6</sub> molecules, in particular benzene.



Indeed, in this study we have identified C<sub>6</sub>H<sub>6</sub> as one of the reaction products, corresponding to the H-loss channel according to eq 2a. Also, we have identified C<sub>5</sub>H<sub>4</sub> consistent with the CH<sub>3</sub>-loss channel as indicated in eq 2b. However, in our study the formation of benzene is not observed. The product detection using multiplexed photoionization mass spectrometry (MPIMS) coupled to tunable vacuum ultraviolet (VUV) synchrotron radiation is intriguing, revealing the presence of cyclic isomers of C<sub>6</sub>H<sub>6</sub> other than benzene, as well as linear isomers. In this paper, we first report low-temperature rate coefficient measurements for the reaction of the ethynyl radical with 1-butyne over

the 74–295 K temperature range in a pulsed Laval nozzle using a chemiluminescence tracer method. The product detection and isomer identification are performed in a slow flow reactor using MPIMS. Time-resolved photoionization efficiency (PIE) curves, i.e., the ion signal as a function of the synchrotron photon energy, for the two product channels are measured. The different product isomers appear as distinct thresholds and are identified according to their ionization energies and the shapes of their Franck–Condon profiles. The implications of these results for polyne formation and their potential role for molecular weight growth chemistry in planetary atmospheres, especially on Titan, and the relationships to combustion reactions, are also discussed.

## 2. Experiment

Two different apparatuses are used to study the reaction of the ethynyl radical ( $C_2H$ ) with 1-butyne ( $C_4H_6$ ). First, low-temperature kinetic measurements are made in a pulsed Laval nozzle apparatus, followed by isomer-resolved product branching studies using a MPIMS coupled to tunable VUV synchrotron radiation at the Advanced Light Source at the Lawrence Berkeley National Laboratory. Experimental details such as error bars for the kinetics measurements, signal-to-noise ratio, and data collection are also discussed. Calculations using the CBS-QB3 composite method<sup>46,47</sup> are performed to determine adiabatic ionization energies of  $C_3H_4$  and  $C_6H_6$  isomers relevant to this work. Photoionization energy curves are computed using the PESCAL program of Ervin.<sup>48,49</sup>

**2.1. Low-Temperature Laval Kinetics.** The rate coefficients are measured in a pulsed Laval nozzle apparatus using laser photolysis and the chemiluminescence tracer method. A detailed description and schematic of the apparatus has been reported elsewhere.<sup>21</sup> In this paper, only the main features of the experiment will be presented. The experimental setup consists of a Laval nozzle mounted on a reservoir block under medium vacuum (0.1–1.0 Torr maintained by a Leybold Heraeus RuVac WS 1000 vacuum pump). Pulsed valves (solenoid Parker valve) are used to inject the gas mixture into the reservoir (1 cm<sup>3</sup> in volume) where the stagnation pressure is monitored by a pressure transducer (Omega PX170 series). The nozzle assembly is mounted on a movable yoke manually driven from outside the chamber. The nozzles used in this study have been characterized in detail.<sup>21</sup>

$C_2H$  radicals are created coaxially within the uniform supersonic expansion by pulsed laser photolysis of acetylene ( $C_2H_2$ ) using an unfocused beam at 193 nm (Lambda Physik COMPex Pro 110 ArF). The diameter of the laser beam is limited by the throat of the Laval nozzle (1 cm in diameter). The laser energy is typically  $\sim 15$  mJ/cm<sup>2</sup> after the divergent section of the nozzle. The concentration of  $C_2H$  radicals inside the flow is monitored by the chemiluminescence tracer method ( $C_2H + O_2 \rightarrow CH(A^2\Delta) + CO_2$ ). The detection zone is situated  $\sim 10$  cm downstream from the exit of the nozzle where light emitted perpendicular to the molecular beam propagation direction is filtered with a  $430 \pm 10$  nm band-pass filter and detected using a photomultiplier tube. The chemiluminescence signal is recorded using a multichannel scaler (Stanford Research Systems, model SR430) in a single-photon-counting mode. A typical decay transient is obtained by accumulating  $\sim 12000$  photolysis laser pulses. The apparatus is run at a 10 Hz repetition rate. Synchronization of the various experimental components is achieved using a digital delay generator (Stanford Research Systems, model DG535).

The  $N_2$ ,  $O_2$ , and  $C_2H_2$  gas flows are supplied directly from cylinders through stainless steel lines and controlled by indi-

vidual calibrated mass flow controllers (MKS Mass-Flo Analog). The 1-butyne cylinder is kept in a cold bath at 278 K to lower its vapor pressure, thus preventing condensation in the gas lines. The gases used in these measurements are as follows: the main carrier gas is  $N_2$  (99.999%),  $C_2H_2$  (99.6%) is used as the radical precursor,  $O_2$  (99.998%), 1-butyne (98% Sigma Aldrich). The acetylene tank is equipped with an activated charcoal cartridge filter to remove acetone, present in the tank as a stabilizing agent, prior to mixing in the main gas flow.

**2.2. Photoionization Mass Spectrometry (PIMS).** The reaction products formed from the reaction of  $C_2H$  with 1-butyne are measured in a slow flow tube reactor coupled to tunable VUV synchrotron radiation at the Advanced Light Source in Berkeley.<sup>50</sup> The MPIMS, building upon the general PIMS design of Slagle and Gutman,<sup>51</sup> has been described in previous studies<sup>17,50,52</sup> and only a brief overview will be given here. The instrument has benefitted from a recent major upgrade: the magnetic sector mass spectrometer described previously has been replaced by an orthogonal accelerated time-of-flight (OA-TOF) mass spectrometer with a superior mass resolution of  $\sim 2000$ . Briefly, the main He gas flow is seeded with the reactants the  $C_2H$  precursor and 1-butyne. All flows are controlled using calibrated mass flow controllers. The pressure inside the flow tube is maintained at 4 Torr (533.3 Pa) by adjusting the pumping speed of the Roots blower using a butterfly valve. At this pressure and room temperature, the total density inside the flow reactor is  $1.3 \times 10^{17}$  cm<sup>-3</sup>. The densities of the  $C_2H$  precursor and 1-butyne are  $2.6 \times 10^{16}$  and  $5.0 \times 10^{14}$  cm<sup>-3</sup>, respectively. The same excimer laser (Lambda Physik COMPex Pro 110 ArF) is used for photolysis but at a lower repetition rate (4 Hz). The measured energy per pulse at the exit of the tube is typically  $\sim 27$  mJ/cm<sup>2</sup>. The unfocused 193 nm laser beam propagates collinearly down the reactor, a 62 cm long quartz tube with a 1.05 cm inner diameter, generating an initial uniform concentration of  $C_2H$  radicals along the tube. The flow velocity inside the reactor is kept constant at  $\sim 4$  m/s. These conditions ensure the photolysis of a fresh gas mixture for each laser pulse. Neutral species escape from a 650  $\mu$ m diameter pinhole on the side of the quartz tube forming an effusive beam that is skimmed by a 0.15 cm diameter skimmer and crossed by tunable VUV synchrotron radiation (8.1–10.1 eV). All ions are monitored simultaneously using an orthogonal accelerated time-of-flight mass spectrometer equipped with a microchannel plate detector. Time-dependent, multiplexed mass spectra are recorded as a function of the synchrotron photon energy to obtain photoionization efficiency curves (PIE). Different structural isomers of the same chemical formula generally have PIE curves that exhibit unique ionization thresholds (ionization energies), shapes (determined by the Franck–Condon overlap between neutral and cation), and absolute intensities (determined by the electronic transition dipole moment).

For the product detection study, the data were taken using 3,3,3-trifluoropropyne ( $CF_3C_2H$ ) as the radical precursor source rather than acetylene ( $C_2H_2$ ) as was used in the Laval nozzle measurements. This choice was made in order to optimize the signal-to-noise ratio of the two product channels in the mass spectrometer for the title reaction. Indeed, previous experiments<sup>17</sup> have shown that  $CF_3C_2H$  is a factor of 2 more efficient than acetylene in producing  $C_2H$  radicals at 193 nm. To ensure a linear response of the ion detector, the average ion count rates are limited to 25 kHz. The photolysis of 1-butyne at 193 nm produces photoproducts (mainly propargyl radicals,  $C_3H_3$ , with an IE of 8.67 eV<sup>53</sup> and methyl radicals,  $CH_3$ ) that are additional species that contribute to the total number of ions arriving on

**TABLE 1: Isomers of C<sub>6</sub>H<sub>6</sub> Relevant to This Work and Their Ionization Energies**

Name	Molecular structure	Ionization energies (eV)	
		Calc. <sup>a</sup>	Exp.
Fulvene		8.40	8.36 <sup>b</sup>
1,3-hexadiene-5-yne		8.63	9.2 <sup>c,d</sup>
DMCB		8.75	8.80 <sup>b</sup>
2-ethynyl-1,3-butadiene		8.95	
3,4-hexadiene-1-yne		8.99	
1,3-hexadiyne		9.37	9.41 <sup>c</sup>
1,5-hexadiyne		9.90	9.90 <sup>b</sup>

<sup>a</sup> This work, CBS-QB3 calculations. <sup>b</sup> Reference 54. <sup>c</sup> Reference 66. <sup>d</sup> Electron impact value minus 0.3 eV as reported in ref 66.

the detector. This unwanted photolysis requires using a minimal amount of 193 nm laser fluence in the flow tube. Therefore to avoid detector saturation and to enhance the product ion signals, CF<sub>3</sub>C<sub>2</sub>H was used as the radical precursor source. Also, above 10.1 eV, the excess reactant, 1-butyne (with an IE of 10.20 eV),<sup>54</sup> in the flow will ionize, increasing the total ion count rate above the allowable range. With the present experimental apparatus, data could not be obtained above the ionization energy of 1-butyne.

The purities of the different gases are as follows: He, 99.9999%; CF<sub>3</sub>C<sub>2</sub>H, 99%; C<sub>2</sub>H<sub>2</sub>, 99.6%; and 1-butyne, 98%. Acetone is removed from the acetylene using a charcoal filter as described in the previous section.

**2.3. Computational Methods.** Adiabatic ionization energies were calculated using the CBS-QB3 composite method of Petersson and co-workers.<sup>46,47</sup> Simulated photoionization efficiency curves, based on the geometries, frequencies, and normal coordinates from the CBS-QB3 calculations, were computed using the PESCAL program of Ervin,<sup>48,49</sup> including full Duschinsky rotation for all totally symmetric modes. The resulting PIE spectra were convolved with a 30 meV fwhm Gaussian function to account for the instrumental resolution. Only the ground electronic states of the cations were included in the calculations, and no attempt was made to predict or model autoionizing resonances. The calculated ionization energies for the C<sub>6</sub>H<sub>6</sub> isomers reported in Table 1 are generally within 0.1 eV of the reported experimental values. Our calculated values for the C<sub>5</sub>H<sub>4</sub> isomers listed in Table 2 are also in good agreement with reported literature values.

### 3. Results

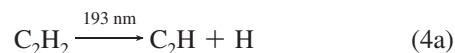
In this section, the low-temperature kinetic measurements will be presented first, followed by the identification of the product channels, identification of the individual isomers, and product branching ratios for the reaction in the slow flow tube reactor coupled to VUV synchrotron radiation detection.

**TABLE 2: Isomers of C<sub>5</sub>H<sub>4</sub> Relevant to This Work and Their Ionization Energies**

Name	Molecular structure	Ionization energies (eV)	
		Calc. <sup>a</sup>	Lit.
1,2,3,4-pentatetraene			8.67 <sup>b</sup>
ethynylallene		9.20	9.22 <sup>c</sup>
methyldiacetylene		9.47	9.5 <sup>d</sup>
1,4-pentadiyne		10.27	10.28 <sup>e</sup>

<sup>a</sup> This work, CBS-QB3 calculations. <sup>b</sup> Reference 54. <sup>c</sup> Reference 62. <sup>d</sup> Reference 75.

**3.1. Low-Temperature Rate Coefficients.** Since the measured percentage depletion for acetylene, as detailed in section 3.2.1 below, by the photolysis laser at 193 nm (see eq 4a) is only 0.5%, it can be assumed that the concentration of the ethynyl radicals, [C<sub>2</sub>H], is much lower than the concentrations of the molecular species, i.e., 1-butyne, acetylene, and oxygen. Therefore, C<sub>2</sub>H radicals are likely to be consumed in the radical–molecule reactions as shown in eqs 4b to 4d rather than radical–radical reactions. A constant amount of O<sub>2</sub> is added in the flow in order to monitor the decay of the C<sub>2</sub>H radical concentration as explained below.



From the reaction scheme outlined above, the rate of change of the concentration of C<sub>2</sub>H radicals can be expressed as

$$\begin{aligned} -\frac{d[\text{C}_2\text{H}]}{dt} &= [\text{C}_2\text{H}](k_{\text{C}_2\text{H}_2}[\text{C}_2\text{H}_2] + k_{\text{O}_2}[\text{O}_2] + k[\text{C}_4\text{H}_6]) \\ &= k_{\text{obs}}[\text{C}_2\text{H}] \end{aligned} \quad (5a)$$

Integrating eq 5a with respect to time yields eq 5b

$$[\text{C}_2\text{H}] = [\text{C}_2\text{H}]_0 \exp[-k_{\text{obs}}t] \quad (5b)$$

where  $k_{\text{C}_2\text{H}_2}$  and  $k_{\text{O}_2}$  are the rate constants for the reaction of the ethynyl radical with acetylene and oxygen, respectively. [C<sub>2</sub>H]<sub>0</sub> is the initial concentration of ethynyl radicals. The rate constant for the reaction of C<sub>2</sub>H with 1-butyne,  $k$ , is determined by plotting the pseudo-first-order rate constants,  $k_{\text{obs}}$ , as a function of the concentration of 1-butyne, [C<sub>4</sub>H<sub>6</sub>], while keeping the concentrations of oxygen and acetylene constant. Chemiluminescence from the electronically excited CH (A<sup>2</sup>Δ)

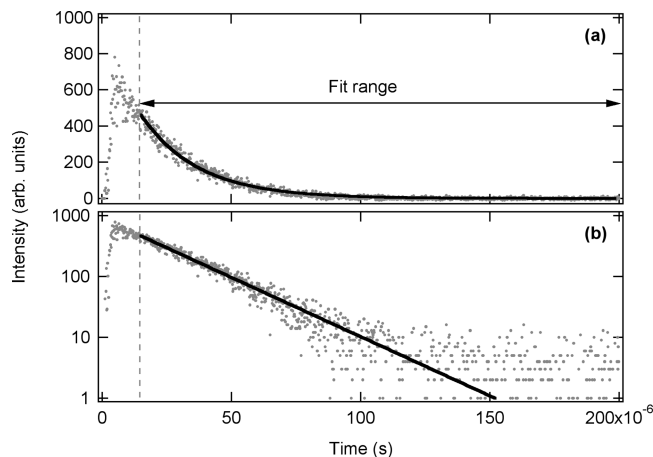


**Figure 1.** Example of net CH ( $A^2\Delta-X^2\Pi$ ) chemiluminescence decay signal at 431.22 nm<sup>56</sup> on (a) a linear scale and (b) a semilogarithmic scale. The solid black line is the single exponential fit of the signal within the range 15–200  $\mu$ s as indicated by the dashed line. The chemiluminescence signal is proportional to the concentration of ethynyl radicals ( $C_2H$ ) under the experimental conditions.

state (see eq 4d) at 431.22 nm<sup>55</sup> is used to monitor the time evolution of the  $C_2H$  radicals in the Laval flow. Because the radiative lifetime for free CH ( $A^2\Delta$ ) radicals (440( $\pm$ 20) ns)<sup>56</sup> is much shorter than the reaction time scale of the ethynyl radicals, a quasi-steady-state approximation can be made for the concentration of CH ( $A^2\Delta$ ). Therefore, it can be assumed that the chemiluminescence emission is directly proportional to the concentration of  $C_2H$  radicals present in the collimated supersonic expansion.

Figure 1 shows a typical decay trace of the chemiluminescence signal as a function of time. The experimental data can be fit by a single exponential function, which confirms the pseudo-first-order approximation made in eqs 5a and 5b. The time interval for the fit for each decay curve is 15  $< t <$  200  $\mu$ s, hence avoiding interference from scattered light and emission produced by the 193 nm laser pulse. This initial 15  $\mu$ s time delay also allows for the quenching of excited  $C_2H$  radicals by nitrogen molecules.<sup>57</sup> As reported previously in the study of the reaction of  $C_2H$  with benzene,<sup>16</sup> the typical quenching time of excited ethynyl radicals in the flow is less than 1  $\mu$ s.

The kinetic measurements are repeated for different concentrations of 1-butene while keeping the concentrations of acetylene and oxygen constant. As shown in Figure 2, the plot of  $k_{obs}$  as a function of the concentration of 1-butene is fit well by a straight line, whose slope is the rate constant,  $k$ , for the  $C_2H + 1$ -butene reaction. This procedure is repeated using different Laval nozzles to examine the temperature dependence of the rate coefficient. At each temperature,  $k_{obs}$  is typically measured for 9–12 different 1-butene densities. The error bars for  $k_{obs}$  are determined to be  $\pm 2\sigma$  of the single exponential fits. The accumulated uncertainties for the concentrations of 1-butene (i.e., 0.5% depletion by the 193 nm laser and 1% error of the actual flow controller) are not shown in Figure 2. The values of the rate coefficients as a function of temperature are summarized in Table 3. The reported uncertainties for these measurements are 20% and are discussed below.

At 193 nm and room temperature, the reported absorption cross section for 1-butene is significant ( $\sim 1 \times 10^{-18}$  cm<sup>2</sup>).<sup>58</sup> As will be discussed in section 3.2.1, our measurements

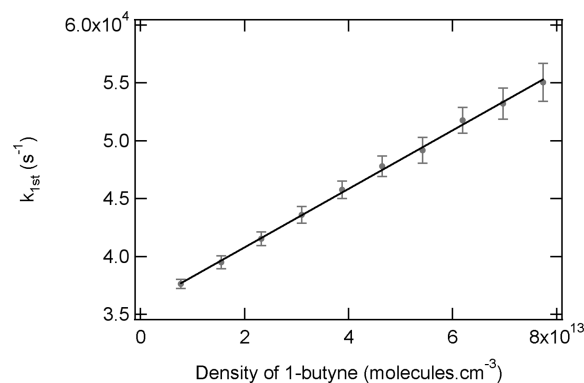


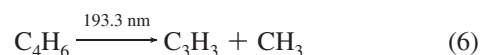
**Figure 2.** Plot of the pseudo-first-order rate constant ( $k_{obs}$ ) as a function of the density of 1-butene inside the flow at 84 K and 0.3 Torr. The black line is a least-squares fit to the experimental values. The error bars are given as  $\pm 2\sigma$  of the single exponential fits for each concentration.

**TABLE 3: Low-Temperature Rate Coefficients of the Reaction of the Ethynyl Radical ( $C_2H$ ) with 1-Butene ( $C_4H_6$ ) Obtained with the Pulsed Laval Nozzle Apparatus<sup>a</sup>**

$T$ (K)	total gas density ( $10^{16}$ cm <sup>-3</sup> )	[ $C_2H_2$ ] ( $10^{14}$ cm <sup>-3</sup> )	[ $O_2$ ] ( $10^{14}$ cm <sup>-3</sup> )	[1-butene] ( $10^{12}$ cm <sup>-3</sup> )	rate constant ( $10^{-10}$ cm <sup>3</sup> s <sup>-1</sup> )
74	2.1	1.2	2.3	4.6–46	2.58 $\pm$ 0.5
84	3.6	2.0	3.9	7.8–77	2.53 $\pm$ 0.5
136	5.6	3.5	7.0	14–136	2.63 $\pm$ 0.5
165	4.6	4.8	4.8	7.5–194	2.43 $\pm$ 0.5
295	3.2	3.8	3.8	4.0–40	2.42 $\pm$ 0.5

<sup>a</sup> The values are given with a total uncertainty of 20%.

indicate that the depletions in 1-butene and acetylene are comparable, i.e.,  $\sim 0.5\%$ . Therefore, we can assume that the destruction of 1-butene at 193 nm is negligible and does not affect the reported densities in the flow. No chemiluminescence signal at  $\sim 430$  nm is detected in the absence of the  $C_2H$  precursor, indicating that the  $C_2H$  photodissociation channel of 1-butene is not significant. We identified  $C_3H_3$  and  $CH_3$  as the main photodissociation products of 1-butene (see eq 6 and section 3.2.1). So we conclude that acetylene photodissociation is the only source of  $C_2H$  radicals and that the single photon photodissociation of 1-butene does not produce  $C_2H$  radicals in significant amounts so as to interfere with the reaction. Again, based on the percentage depletion measurements (radical species) and the actual densities of the reagents (molecular species) in the flow, the probability of radical–radical removal of  $C_2H$  is negligible compared to removal by radical + stable molecule reactions.



Decreasing the energy of the photolysis laser by a factor of 2 did not change the measured rate constants significantly. Fitting the present data to a temperature-dependent rate expression yields  $k = (2.4 \pm 0.5) \times 10^{-10} (T/295 \text{ K})^{-(0.04 \pm 0.03)}$  cm<sup>3</sup> molecule<sup>-1</sup> s<sup>-1</sup>. However, as the temperature dependence is essentially negligible within the experimental uncertainties, we recommend for kinetic modeling that the average rate coefficient,  $k = 2.5 \times 10^{-10}$  cm<sup>3</sup> molecule<sup>-1</sup> s<sup>-1</sup>, should be taken with a total uncertainty of 20%.

**3.2. Tunable VUV Isomer-Specific Product Detection.** The goal of product detection studies coupled with kinetics

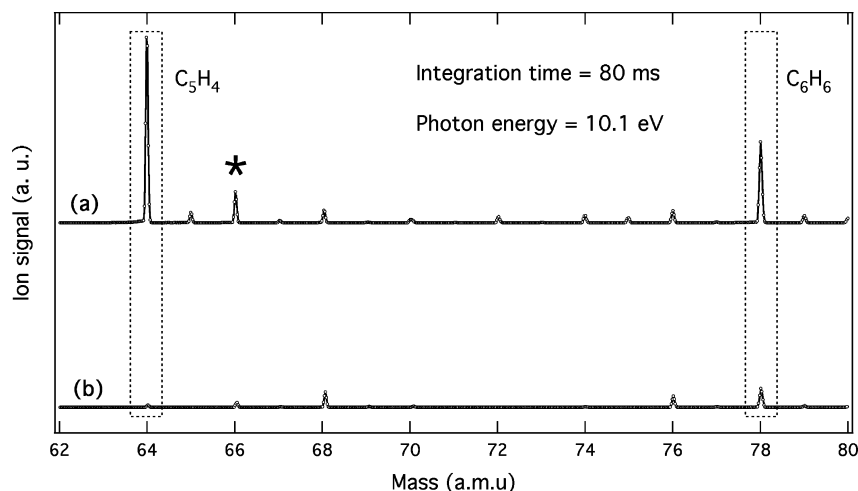


**Figure 3.** Mass spectra at 10.1 eV photoionization energy with (a) the C<sub>2</sub>H precursor and 1-butyne and (b) only 1-butyne flowing under the same exact conditions. Two masses show a significant rise as the C<sub>2</sub>H precursor is added, i.e.,  $m/z = 64$  and  $m/z = 78$  which are consistent with the CH<sub>3</sub>- and H-loss channels of the reaction, respectively. The contribution of the 193 nm photoproducts of 1-butyne to the  $m/z = 78$  product channel of the reaction is discussed in section 3.2.1. Note that the contribution to the ion signal at  $m/z = 66$  (\*) is due to the reaction of the ethynyl radical with butene (C<sub>4</sub>H<sub>8</sub>) present as a small contaminant in the flow.

measurements is to identify and estimate branching ratios for the products of the reaction between the ethynyl radical with 1-butyne. In this respect, the reaction has been studied at 295 K and 533 Pa in the slow flow reactor using MPIMS with tunable VUV synchrotron radiation. Both time- and energy-resolved data have been collected as described in section 2.2. Mass spectra as a function of the ionization energy are retrieved from the raw data by integrating over the whole reaction time scale of 80 ms. Note that mass spectra are also taken for 20 ms before the pulsing of the photolysis laser for background subtraction. In this way, identification by  $m/z$  ratio of all species involved in the reaction is obtained. Then, for a given mass, the evolution of the ion signal as a function of: (1) time, which reveals the chemical nature of the species, i.e., precursor, photolysis product, primary reaction product, or secondary reaction product, and (2) photon energy, which helps to determine and distinguish between different isomers, is analyzed. Indeed, the presence of different isomers with different ionization energies is revealed as different thresholds and shapes in the PIE curves.

Figure 3a shows a mass spectrum with the radical precursor and the reactant, 1-butyne, flowing in the buffer gas and Figure 3b shows a second mass spectrum with only 1-butyne, both acquired at 10.1 eV and integrated over 80 ms of reaction time, with the 193 nm photolysis laser and the same density of 1-butyne. Both mass spectra are background subtracted. Two mass peaks show a significant increase when the C<sub>2</sub>H precursor is added:  $m/z = 64$  and  $m/z = 78$ . Given the measured rate coefficient for the reaction of C<sub>2</sub>H with 1-butyne, the concentration of the reactants, and the instrumental time resolution, it is not possible to measure the rise time of these two products. However, the observed instrument-limited rise time after the photolysis laser pulse and the fact that the ion signal for both masses remains constant at later times is consistent with the formation of a closed-shell, unreactive species. After careful inspection of the mass spectra in Figure 3, the following observations can be made:

1. The ion signal at  $m/z = 64$  (C<sub>5</sub>H<sub>4</sub>) is almost entirely due to the simultaneous presence of C<sub>2</sub>H, created by the photolysis laser, and 1-butyne. This result is consistent with the C<sub>5</sub>H<sub>4</sub> + CH<sub>3</sub> product channel for the title reaction.

2. The ion signal at  $m/z = 78$  (C<sub>6</sub>H<sub>6</sub>) shows a significant enhancement (by a factor of ~6) when the radical precursor is

added to the flow. This result is consistent with the C<sub>6</sub>H<sub>6</sub> + H product channel for the title reaction. But, it is noted that there is some background contribution to the  $m/z = 78$  ion signal in the absence of the C<sub>2</sub>H radical precursor.

Before analyzing these two ion signals, it is important to identify any side reactions that might interfere with the two product channels (see section 3.2.1). As mentioned in section 3.1, 1-butyne has a significant photodissociation cross section at 193 nm, giving rise to additional radical species that can react with the reagents in the flow. In order to evaluate the contribution of these photodissociation products and extract the true signals for the title reaction, two separate sets of data, with the same concentration of 1-butyne in the flow, were collected (with and without the radical precursor). As seen in Figure 3b, the contribution of 1-butyne photodissociation products to  $m/z = 64$  ion signal is negligible, showing that C<sub>5</sub>H<sub>4</sub> is indeed the product of the CH<sub>3</sub>-loss channel for the title reaction. The PIE curve is analyzed in section 3.2.2. However, the side reactions that produce the  $m/z = 78$  ion signal are not negligible. Therefore, we extracted from the two sets of data a PIE curve for  $m/z = 78$  ions with (◆) and without (⊗) the radical precursor (see Figure 4 and caption for details). In this way, the increase in the ion signal, i.e., (◆) minus (⊗), is the contribution of products from the title reaction products to the  $m/z = 78$  ion signal. The result is a PIE curve for the C<sub>6</sub>H<sub>6</sub> product channel, which is analyzed in section 3.2.3. Estimates of branching ratios are also derived for each product channel. Note that complete data sets in our experiment are limited to VUV photon energies between 8.2 and 10.1 eV due to experimental limitations as detailed in section 2.2.

**3.2.1. Photodissociation and Photoproducts of Reactants at 193 nm.** Figure 5 shows the photodepletion measurements of (a) 1-butyne, (b) acetylene, and (c) 3,3,3-trifluoropropyne recorded at 193 nm. These experiments have been done in order to quantify the photodepletion of 1-butyne by the laser and to choose between acetylene and 3,3,3-trifluoropropyne for the C<sub>2</sub>H precursor. Each data set is fit to a step function after the pulsing of the laser at 20 ms. The average laser energy is ~27 mJ/pulse in all experiments, and the measured percentage depletion as well as the composition of the gas mixtures are reported in Table 4. From these measurements, it can be noted that the photodepletion of 1-butyne and acetylene are comparable, i.e., 0.45% and 0.47%, respectively. As expected,<sup>59</sup> the photodis-



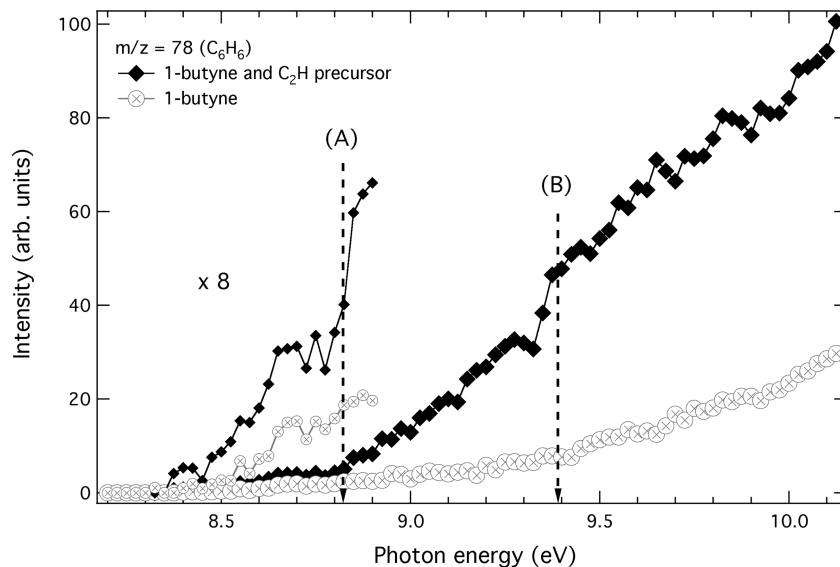


**Figure 4.** Photoionization efficiency curves for  $m/z = 78$  ( $C_6H_6$ ) mass channel with ( $\blacklozenge$ ) and without ( $\otimes$ ) the  $C_2H$  precursor. Both PIE curves have been recorded with the same concentration of 1-butynes in the total gas flow. The photodissociation of 1-butynes at 193 nm produces propargyl radicals ( $C_3H_3$ ) that subsequently react with 1-butynes to form  $C_6H_6 + CH_3$ . In presence of  $C_2H$  radicals, the ion signal is enhanced (typically by a factor of  $\sim 6$ ) which is consistent with the formation of  $C_6H_6$  as a product of the reaction of  $C_2H$  radicals with 1-butynes. Two thresholds are identified and indicated by dashed arrows: (A) around 8.8 eV photoionization energy as shown in the region between 8.1 and 8.9 eV (zoom  $\times 8$ ) and (B) around 9.4 eV. The identification of the different isomers  $C_6H_6$  is discussed in section 3.2.3.

sociation of 3,3,3-trifluoropropyne is more efficient by a factor of 2 (0.83%) compared to acetylene. In addition to the high yield of  $C_2H$  radicals, the photolysis of  $CF_3C_2H$  leaves behind less reactive  $CF_3$  radicals compared to H-atoms from acetylene. We have used 3,3,3-trifluoropropyne as the  $C_2H$  radical precursor in order to optimize the signal for the two product channels because it allows us to increase the concentration of ethynyl radicals while keeping the 193 nm laser energy low enough to minimize 1-butynes photodissociation.

As mentioned in the previous section, 1-butynes has a significant photodissociation cross section at 193 nm. It is most likely that the photoproducts are radical species that can further react with 1-butynes to yield stable hydrocarbons. These products can interfere with the product channels of the title reaction. Quantifying the contribution of these photodissociation products of the alkyne to the ion signals is therefore crucial in our experiment for accurate isomer-specific product detection. We have identified methyl ( $CH_3$ , IE = 9.843 eV)<sup>60</sup> and propargyl ( $C_3H_3$ , IE = 8.67 eV)<sup>53</sup> as the two main radical species formed from the 193 nm photolysis of 1-butynes (not shown on mass spectra of Figure 3).  $CH_3$  radicals can react with  $C_4H_6$  or  $CF_3C_2H$  molecules in the flow. However, it is unlikely that the products of the reaction will contribute to the ion signal at either  $m/z = 64$  ( $C_3H_4$ ) or 78 ( $C_6H_6$ ). On the other hand,  $C_3H_3$  radicals could react with  $C_4H_6$  to produce  $C_6H_6$  (e.g., benzene) by losing a  $CH_3$  radical according to eq 7a. The formation of  $C_5H_4$  (e.g., methylidyneacetylene) is found to be endothermic (eq 7b) and therefore not favorable.  $C_3H_3$  radicals could also react with  $CF_3C_2H$  to produce  $C_5H_4$  by losing a  $CF_3$  radical.

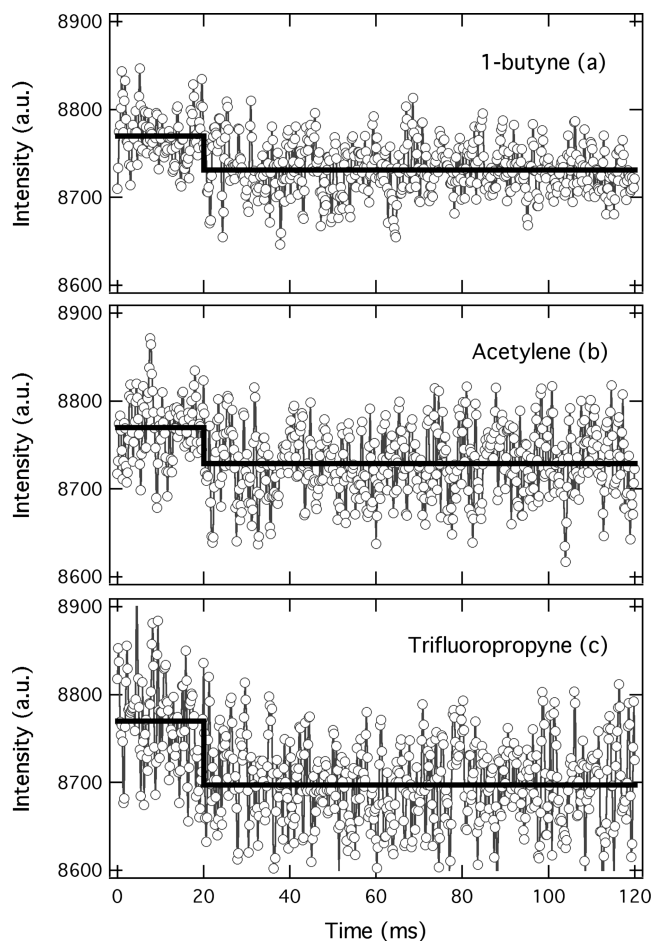
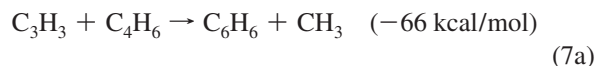


**Figure 5.** Measurements of the photodepletion of (a) 1-butynes, (b) acetylene, and (c) 3,3,3-trifluoropropyne at 193 nm. All gases are seeded in He buffer gas at the following compositions: 0.1% for both 1-butynes and acetylene and 1% for 3,3,3-trifluoropropyne. The excimer laser energy used for the three different species is typically  $\sim 27$  mJ/cm<sup>2</sup>. All data sets are fit by a step function (solid black line) after the laser is pulsed at 20 ms. The percentage depletion is reported in Table 4.

**TABLE 4: Percent Photodepletion of Acetylene, 3,3,3-Trifluoropropyne and 1-Butyne at 193 nm at a Laser Energy  $\sim$ 27 mJ/pulse<sup>a</sup>**

molecule	formula	IE (eV)	% in He buffer gas	% depletion
acetylene	C <sub>2</sub> H <sub>2</sub>	11.40 <sup>76</sup>	0.1	0.47
3,3,3-trifluoropropyne	CF <sub>3</sub> C <sub>2</sub> H	11.96 <sup>54</sup>	1.0	0.83
1-butyne	C <sub>4</sub> H <sub>6</sub>	10.20 <sup>54</sup>	0.1	0.45

<sup>a</sup> The experimental data are fit to a step function after the laser is pulsed, i.e., at  $t = 20$  ms (see Figure 5 and section 3.2.1).

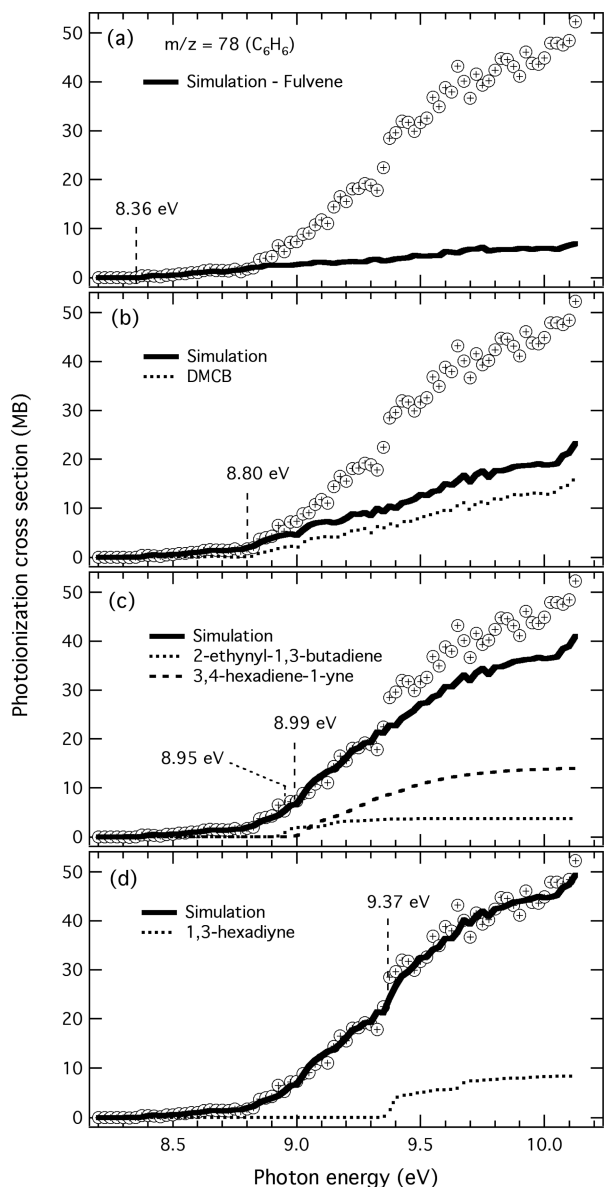
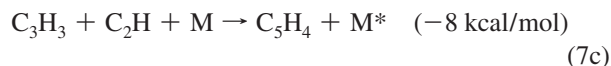
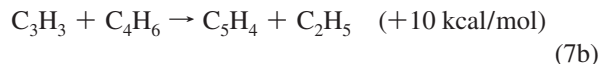


**Figure 6.** Photoionization efficiency curve ( $\oplus$ ) of  $m/z = 78$  product ion. The individual contributions of the C<sub>6</sub>H<sub>6</sub> isomers (dotted and dashed lines) are shown, as well as the cumulative simulation (thick black line). The adiabatic ionization energies for each isomer are also labeled: (a) fulvene, (b) DMCB, (c) 2-ethynyl-1,3-butadiene, 3,4-hexadiene-1-yne, and (d) 1,3-hexadiyne. The production of the aromatic six-membered ring isomer, benzene, is most probably negligible as no sharp characteristic onset is observed around 9.23 eV (see section 3.2.3). The PIE curve is normalized to the total estimated cross section of an average mixture of 18% of fulvene, 32% of DMCB, 8% of 2-ethynyl-1,3-butadiene, 28% of 3,4-hexadiene-1-yne, and 14% of 1,3-hexadiyne using the estimated photoionization cross sections at 10 eV reported in Table 6.



However, reactions of propargyl with closed-shell molecules are relatively slow. On the other hand, recombination of two propargyl radicals could be a source of C<sub>6</sub>H<sub>6</sub> (eq 1). Similarly, C<sub>3</sub>H<sub>3</sub> + C<sub>2</sub>H could be a source of C<sub>5</sub>H<sub>4</sub> as shown in eq 7c, and it is unlikely that C<sub>2</sub>H + C<sub>2</sub>H will contribute to the ion signal at either  $m/z = 64$  (C<sub>5</sub>H<sub>4</sub>) or 78 (C<sub>6</sub>H<sub>6</sub>). At the pressure of the present experiments (533 Pa), it is expected that stabilization dominates the propargyl + propargyl reaction, with only about 10<sup>-3</sup> branching to phenyl + H.<sup>61</sup> On the basis of these considerations, we identify C<sub>3</sub>H<sub>3</sub> + C<sub>3</sub>H<sub>3</sub> as the main side reaction contributing to the  $m/z = 78$  ion signal for pure 1-butyne photolysis. By flowing only the C<sub>2</sub>H precursor in the buffer gas, we verified that no contribution of trifluoropropyne photoproducts to the two mass channels of interest was observed.

Figure 4 shows the PIE curves with and without the C<sub>2</sub>H precursor for  $m/z = 78$  ion signal. Assuming that the main interference in the  $m/z = 78$  ion signal is the product of C<sub>3</sub>H<sub>3</sub> + C<sub>3</sub>H<sub>3</sub> (eq 1) and that C<sub>6</sub>H<sub>6</sub> is one product of the C<sub>2</sub>H + 1-butyne reaction as shown in eq 4b and discussed above, we can subtract the  $m/z = 78$  ion signal resulting from propargyl recombination obtained without C<sub>2</sub>H radicals present from the total ion signal for  $m/z = 78$  when C<sub>2</sub>H radicals are present. This process yields the PIE curve for the title reaction, which is shown in Figure 6. For  $m/z = 64$  (C<sub>5</sub>H<sub>4</sub>), the PIE curve is shown in Figure 7. In the sections to follow, these two PIE curves are analyzed and estimates of branching ratios are derived for the C<sub>5</sub>H<sub>4</sub> and C<sub>6</sub>H<sub>6</sub> product channels.

**3.2.2. C<sub>5</sub>H<sub>4</sub> from the Reaction of the Ethynyl Radical with 1-Butyne.** Figure 7 shows the PIE curve for the C<sub>5</sub>H<sub>4</sub> mass channel for the reaction of the ethynyl radical with 1-butyne. In our analysis of the observed PIE curve below, literature and calculated values of the ionization energies of the C<sub>5</sub>H<sub>4</sub> isomers are taken from the work of Goulay and co-workers<sup>17</sup> and Hansen and co-workers.<sup>62</sup> Because the absolute photoionization cross sections are not available for all of the C<sub>5</sub>H<sub>4</sub> isomers, we have used the single point estimates of photoionization cross sections already reported.<sup>17</sup> Hansen and co-workers<sup>62</sup> performed Franck–Condon simulations for ethynylallene (CH<sub>2</sub>CCHCCH), methylidyneacetylene, and 1,4-pentadiyne in their study of C<sub>5</sub>H<sub>x</sub> isomers<sup>62</sup> for an assumed temperature of 300 K. The simulated photoionization efficiency curves are in very good agreement with their experimental data for the C<sub>5</sub>H<sub>4</sub> isomers. In the absence of any reference data for these isomers, these simulated curves are used to fit our experimental data.

The observed PIE curve shown in Figure 7 can be fit between 8.1 and 9.9 eV by a weighted sum of Franck–Condon based simulations for the two most stable isomers of C<sub>5</sub>H<sub>4</sub>, i.e., ethynylallene and methylidyneacetylene. Since no threshold in the ion signal is observed at 8.67 eV, we conclude that the 1,2,3,4-pentatetraene isomer is not produced by the reaction. The first sharp rise in the ion signal at 9.15 eV is attributed to the presence of ethynylallene. The only reported adiabatic ionization energy for this isomer is 9.22 eV using QCISD(T) calculations,<sup>62</sup> in good agreement with our calculated value of 9.20 eV. The solid black line in Figure 7a indicates the fit including only the contribution of the CH<sub>2</sub>CCHCCH isomer. Note that the calculated photoionization efficiency curve increases slowly above 9.25 eV with a step around 9.5 eV,<sup>62</sup> almost coinciding with

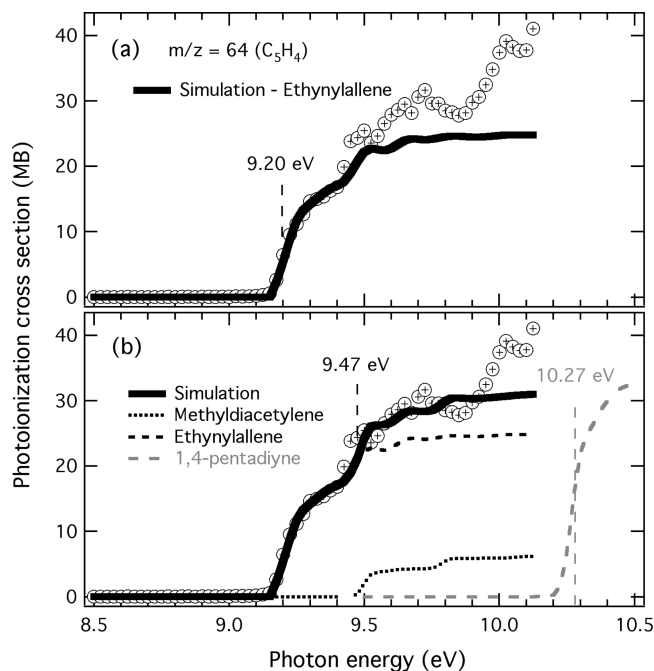


**Figure 7.** Photoionization efficiency curve ( $\oplus$ ) of  $m/z = 64$ . Note that no threshold in the ion signal is observed at 8.67 eV, indicating that no 1,2,3,4-pentatetraene is produced in the reaction. (a) A single contribution of ethynylallene cannot account for the observed ion signal in the 8.2–10.1 photon range. (b) The individual contributions of ethynylallene (dashed line) and methylidyacetylene (dotted line) are shown. The ion signal can be fit by a sum of weighted contributions of Franck–Condon simulations<sup>62</sup> at 300 K of the two most stable  $C_5H_4$  isomers as shown by the thick black line. The calculated PIE curve of 1,4-pentadiyne (gray dashed line) is also indicated. Due to experimental limitations, the presence or absence of 1,4-pentadiyne (IE = 10.27 eV)<sup>62</sup> cannot be probed. The signal is normalized to the total estimated photoionization cross section at 9.8 eV using estimated values reported in Table 5.

**TABLE 5: Estimated Photoionization Absorption Cross Sections of  $C_5H_4$  Isomers Identified in the PIE Curve Shown in Figure 7 (see Section 3.2.2)**

$C_5H_4$ isomers	photon energy (eV)		
	9.4	9.8	10.4
ethynylallene <sup>a</sup>	25 MB	30 MB	30 MB
methylidyacetylene <sup>a</sup>		30 MB	35 MB
1,4-pentadiyne <sup>a</sup>			30 MB

<sup>a</sup> Reference 17.

the next threshold in the ion signal. However, the fit assuming only ethynylallene contributes to the PIE curve between 8.1 and 9.9 eV is fairly poor, which suggests the presence of an additional isomer. It follows that the threshold at 9.5 eV is most certainly due to the presence of methylidyacetylene. Moreover, there is a good agreement between the simulated PIE curve and the actual experimental data, as seen in Figure 7b, when the contribution from methylidyacetylene is taken into account in the overall fit up to 9.9 eV.

The observed signal as a function of photon energy,  $S(E)$ , is proportional to the sum of the individual photoionization cross sections,  $\sigma_i(E)$ , weighted by the mole fraction of each  $C_5H_4$  isomer,  $X_i$ , as indicated in eq 8. Reliable estimates for the photoionization cross sections can be obtained as described<sup>17</sup> using a semiempirical model by Bobeldijk and co-workers.<sup>63</sup> With the reported values,<sup>17</sup> we can estimate a ratio for ethynylallene/methylidyacetylene of approximately 4:1 for the reaction of the ethynyl radical with 1-butyne.

$$S(E) \propto \sigma_{\text{total}}(E) = \sum_{i=1}^m \sigma_i(E) X_i \quad (8)$$

Due to experimental limitations as described in section 2.2, a complete set of data above 10.125 eV could not be obtained. Therefore, in our experiment we cannot probe the presence or absence of 1,4-pentadiyne (IE = 10.27 eV).<sup>54</sup> The gray dashed line in Figure 7b represents the calculated PIE curve of 1,4-pentadiyne. The residual of the fit with ethynylallene and methylidyacetylene in Figure 7 suggests the presence of another ionization threshold near 9.95 eV. However, as seen by Goulay and co-workers<sup>17</sup> in the reaction of  $C_2H$  + propyne, the ion signal for  $m/z = 64$  should follow a slight linear increase as a function of photon energy above 9.8 eV when only ethynylallene and methylidyacetylene are present. This would suggest that the observed threshold in our experiment might be due to the presence of another  $C_5H_4$  isomer. Nevertheless, on the basis of the molecular structure of methylidyacetylene (IE = 9.47 eV) and 1,4-pentadiyne (IE = 10.27 eV), i.e., both molecules have two triple bonds, compared with ethynylallene (with a lower IE = 9.20 eV), which has two double bonds and a single triple bond, it is hard to propose a rational structure of a linear  $C_5H_4$  isomer that could possibly have an ionization energy around 10 eV. Also, this threshold feature could be explained by dissociative ionization of a heavier molecule or the presence of an electronically excited state of  $C_5H_4^+$ . Again, in the absence of a complete set of data at higher photon energies, we can only quantify the isomeric distribution of methylidyacetylene and ethynylallene.

The fit of the PIE curve, indicated as a thick black line is shown in Figure 7b, is the sum of the individual contributions (FC simulations) of ethynylallene (dashed line) and methylidyacetylene (dotted line). The PIE curve is normalized to the total estimated cross section at 9.8 eV of an average mixture of 82( $\pm$ 15)% of ethynylallene and 18( $\pm$ 15)% of methylidyacetylene using estimated photoionization cross sections reported in Table 5.

**3.2.3.  $C_6H_6$  from the Reaction of the Ethynyl Radical with 1-Butyne.** Figure 6 shows the photoionization efficiency curve for  $m/z = 78$  ( $C_6H_6$ ) mass channel, from the reaction of the  $C_2H$  radical and 1-butyne. Relative photoionization efficiency curves are used when available for some of the  $C_6H_6$  isomers considered herein.<sup>64</sup> The 8.2–9.1 eV range exhibits a very slow monotonic rise in the ion signal. At 8.36 eV a first threshold is observed, corresponding to the ionization energy of the cyclic five-membered  $C_6H_6$  isomer, fulvene. Furthermore, the onset of the signal can be replicated by its relative PIE curve.<sup>64</sup> A second threshold is identified at 8.8 eV. In this portion of the PIE curve, a single contribution by fulvene cannot account for the observed signal as shown in Figure 6b. This second onset corresponds to the ionization energy of 3,4-dimethylenecyclobut-1-ene (DMCB), a four-membered cyclic isomer of  $C_6H_6$ . A good fit is obtained with a weighted sum including the relative PIE curves for fulvene and DMCB, further confirming the presence of the latter. Using estimated values<sup>44</sup> for the photoionization absorption cross sections of these two species (see Table 6), these isomers are formed in an approximate ratio of 1:2.

The residual of the fit including fulvene and DMCB (thick black line in Figure 6b) indicates a small feature between 8.9 and 9.4 eV followed by a sharp increase in the photoionization signal around 9.4 eV. In this energy range, there are four possible  $C_6H_6$  isomers: 2-ethynyl-1,3-butadiene (IE = 8.95 eV), 3,4-hexadiene-1-yne (IE = 8.99 eV), benzene (IE = 9.24 eV),<sup>65</sup>

**TABLE 6: Estimated Photoionization Absorption Cross Sections of C<sub>6</sub>H<sub>6</sub> Isomers (see Section 3.2.3) Identified in the PIE Curve Shown in Figure 6**

C <sub>6</sub> H <sub>6</sub> isomers	photon energy (eV)			
	8.6	8.9	9.2	10
fulvene	6 MB	14 MB	18 MB	35 MB
3,4-dimethylenecyclobut-1-ene		5 MB	15 MB	40 MB
2-ethynyl-1,3-butadiene			42 MB	50 MB
3,4-hexadiene-1-yne			18 MB	50 MB
1,3-hexadiyne				59 MB

and 1,3-hexadiyne (IE = 9.41 eV<sup>66</sup>). The relative PIE curve of benzene is well-known<sup>64</sup> while those of 2-ethynyl-1,3-butadiene, 3,4-hexadiene-1-yne, and 1,3-hexadiyne have been computed as discussed in section 2.3. Benzene has a very distinctive onset and characteristic PIE curve<sup>64</sup> shape that does not seem to match with the feature observed around 9.3 eV. Since the small onset occurs before the well-defined ionization potential of benzene, the small feature is more likely related to 2-ethynyl-1,3-butadiene and 3,4-hexadiene-1-yne. Indeed, a good fit (solid black line) of the experimental data is obtained up to 9.35 eV when a weighted contribution of 2-ethynyl-1,3-butadiene (dotted line) and 3,4-hexadiene-1-yne (dashed line) is included as shown in Figure 6c. Note that the calculated IE of 1,3-hexadiene-5-yne (8.63 eV) is found to be 0.6 eV lower than the reported experimental value (9.3 eV), which is an estimated value from electron impact measurements.<sup>66</sup> No threshold in the ion signal is observed around 8.6 eV indicating that 1,3-hexadiene-5-yne is not produced in significant amounts. Although it is therefore difficult to firmly quantify benzene in our experiment, it is probably not produced in significant quantities.

It is likely that the next threshold observed at 9.4 eV is due to the linear C<sub>6</sub>H<sub>6</sub> isomer, 1,3-hexadiyne. Additional thresholds above 9.4 eV are not observed, indicating that 1,4-hexadiyne and 1,5-hexadiyne are also negligible reaction products. The fit of the PIE curve, indicated as a thick black line, is the sum of the individual contributions (FC simulations) of fulvene, DMCB, 2-ethynyl-1,3-butadiene, 3,4-hexadiene-1-yne and 1,3-hexadiyne. The PIE curve is normalized to the total estimated cross section of an average mixture of 18% of fulvene, 32% of DMCB, 8% of 2-ethynyl-1,3-butadiene, 28% of 3,4-hexadiene-1-yne, and 14% of 1,3-hexadiyne using the estimated photoionization cross sections at 10 eV (see Table 6). Within experimental uncertainties, an upper limit of 10% is estimated for benzene production.

#### 4. Discussion

In this paper, we present the only experimental work reporting both low-temperature kinetics and room-temperature product detection of the ethynyl radical (C<sub>2</sub>H) with a C<sub>4</sub> molecule, 1-butyne. The rate coefficient measurements, within experimental uncertainty, exhibit almost no temperature dependence in the 74–295 K range as shown in Figure 8. Using photoionization mass spectrometry coupled to tunable VUV synchrotron radiation, we have direct information about the product channels involved (4 Torr, 295 K) and we have been able to determine and distinguish between the different isomers present. We discuss below the probable mechanism for the reaction of the C<sub>2</sub>H radical and 1-butyne and the possible implications for the photochemistry of the outerplanets, especially the Saturnian moon Titan.

##### 4.1. Temperature Dependence and Reaction Mechanism.

It is worthwhile to compare the measured rate coefficients of the reaction of the C<sub>2</sub>H radical with 1-butyne (or ethylacetylene)

with the smaller alkynes, i.e., acetylene (C<sub>2</sub>H<sub>2</sub>) and propyne (or methylacetylene, C<sub>3</sub>H<sub>4</sub>). Figure 8 shows a plot of the rate constants for the title reaction as a function of temperature along with analogous measurements for acetylene and propyne obtained in a collaborative work between Leone and co-workers and Sims and co-workers.<sup>13,25</sup> As pointed out by Sims and co-workers,<sup>13</sup> the results obtained independently using a pulsed and a continuous Laval nozzle are in satisfactory agreement. Moreover, a general rule of thumb is derived by taking the measured rate coefficient for acetylene ( $k_{\text{C}_2\text{H}_2} = 1.9 \times 10^{-10}$  cm<sup>3</sup> molecule<sup>-1</sup> s<sup>-1</sup> at  $T \approx 50$  K) and its ionization energy of 11.4 eV as a reference to estimate low-temperature rate coefficients of C<sub>3</sub> and C<sub>4</sub> alkenes and alkynes as a function of their ionization energies. With this correlation, it is expected that the rate constant should increase with molecular mass (or decreasing ionization energy) for the corresponding alkenes, alkynes, dienes, and diynes. As shown in Figure 8, the measured rate coefficient with C<sub>4</sub>H<sub>6</sub> ( $k = 2.6 \times 10^{-10}$  cm<sup>3</sup> molecule<sup>-1</sup> s<sup>-1</sup> at  $T \approx 74$  K) is higher than C<sub>2</sub>H<sub>2</sub> but comparable with C<sub>3</sub>H<sub>4</sub> and is therefore in agreement with the expected trend. It should be noted that in the temperature range 70–100 K, the reaction with the C<sub>2</sub>H radical is rapid and close to the collision-determined limit. Our data are also consistent with the measured rate coefficients of the C<sub>2</sub>H with 1,3-butadiene reaction.<sup>39</sup> Indeed, our rate constant is slightly lower than the C<sub>4</sub> diene ( $k_{\text{C}_4\text{H}_6} = 2.9 \times 10^{-10}$  cm<sup>3</sup> molecule<sup>-1</sup> s<sup>-1</sup> at  $T \approx 104$  K), which is in agreement with the lower ionization energy of 9.072 eV<sup>67</sup> for 1,3-butadiene. No measurements of rate coefficients for the reactions of C<sub>2</sub>H and the two other linear C<sub>4</sub>H<sub>6</sub> isomers, i.e., 1,2-butadiene (IE = 9.03 eV<sup>68</sup>) and 2-butyne (IE = 9.59 eV<sup>54</sup>) are available. However, our results combined with previous studies<sup>39</sup> suggest that the rate coefficients for these reactions should be comparable. The reaction of the C<sub>2</sub>H radical with linear C<sub>4</sub>H<sub>6</sub> isomers is most probably barrierless, showing almost no temperature dependence, and a rate coefficient can be estimated to be in the range  $(2.5\text{--}3.0) \times 10^{-10}$  cm<sup>3</sup> molecule<sup>-1</sup> s<sup>-1</sup>.

Before the possible mechanism for the reaction is considered, it is useful to compare the energetics of propargyl recombination,<sup>61</sup> which has been identified as a benzene formation pathway in fuel-rich flames.<sup>44</sup> Figure 9 shows the heats of reaction ( $\Delta H_r^\circ$  in kcal/mol) in which the three most stable C<sub>6</sub>H<sub>6</sub> isomers, i.e., DMCB, fulvene, and benzene, are produced. The three-body recombination of two propargyl radicals leading to C<sub>6</sub>H<sub>6</sub> isomers is more exothermic (~38 kcal/mol) compared to the formation of the same isomers through the H-loss channel of C<sub>2</sub>H + 1-butyne reaction. In the latter case, the C<sub>6</sub>H<sub>6</sub> products are left with less internal energy and as a consequence further isomerizations on the C<sub>6</sub>H<sub>6</sub> potential energy surface to form more stable isomeric structures, e.g., DMCB to fulvene or fulvene to benzene, are probably less facile. In fact, most of the isomerization transition states calculated by Miller and Klippenstein are predicted to be energetically inaccessible for the C<sub>6</sub>H<sub>6</sub> product of the C<sub>2</sub>H + 1-butyne reaction, so the isomerization steps that determine the product distribution most likely take place on the C<sub>6</sub>H<sub>7</sub> surface. The heats of formation of methyldiacetylene (–39 kcal/mol), diacetylene (–36 kcal/mol), and DMCB (–43 kcal/mol) for the title reaction are all comparable. Because methyldiacetylene and DMCB are detected in the reaction at room temperature, the C<sub>2</sub>H<sub>5</sub>-loss channel to form C<sub>4</sub>H<sub>2</sub> (diacetylene) is presumably also accessible. However, the ionization energy of diacetylene, 10.17 eV, is too close to that of 1-butyne, and we cannot operate at high enough photon energies to directly probe this channel in our experiment.

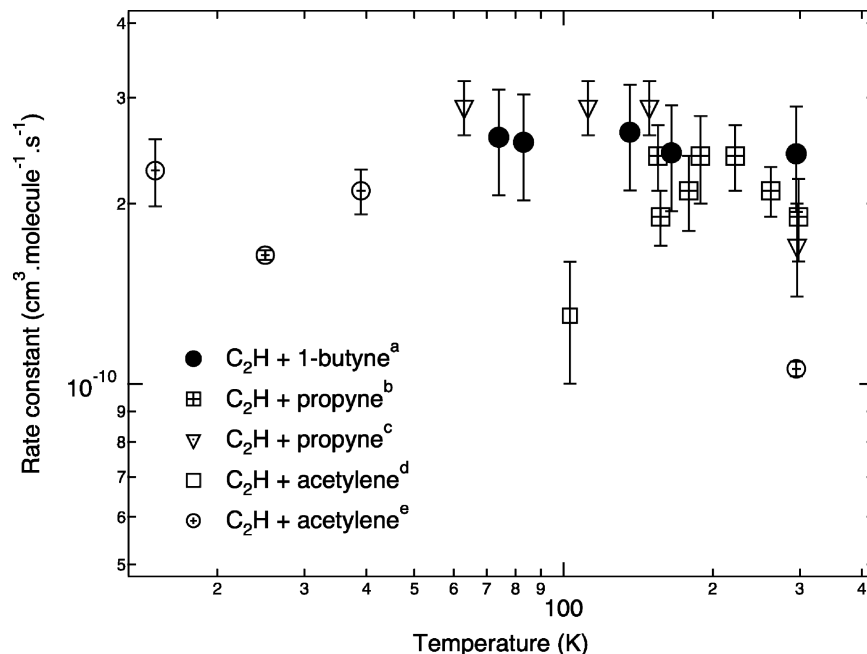


**Figure 8.** Comparison between the measured rate constant for the reactions of the ethynyl radical with 1-butyne (<sup>a</sup>this work) and the smaller alkynes: propyne (<sup>b</sup>Leone and co-workers<sup>25</sup> and <sup>c</sup>Sims and co-workers<sup>13</sup>) and acetylene (<sup>d</sup>Leone and co-workers<sup>24</sup> and <sup>e</sup>Sims and co-workers<sup>33</sup>).

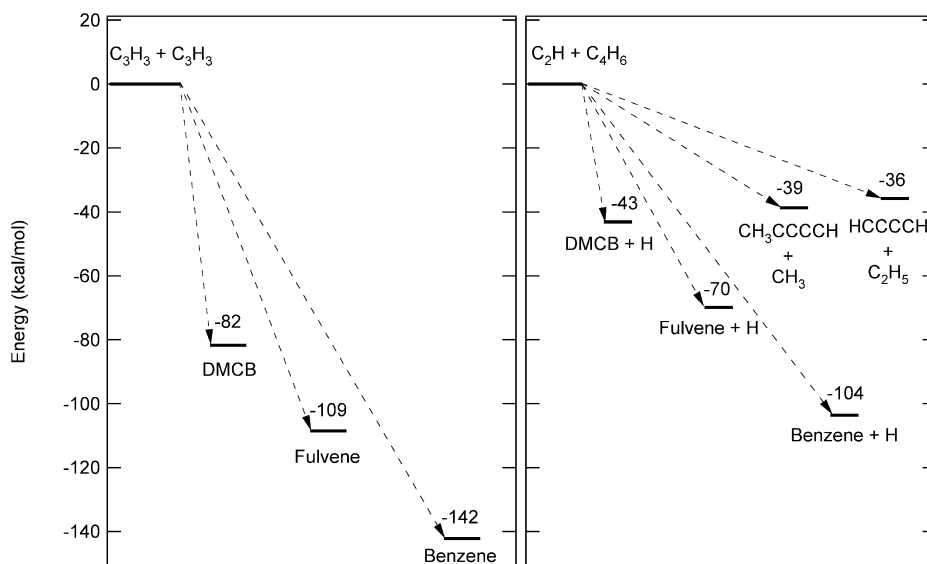


**Figure 9.** A comparison of the thermochemistry of the  $C_3H_3 + C_3H_3$  and  $C_2H + 1\text{-butyne}$  reactions. The standard heats of reaction (kcal/mol) leading to the three most stable  $C_6H_6$  isomers, i.e., DMCB, fulvene, and benzene, are shown in both cases. The difference in internal energy accompanying benzene is  $\sim 38$  kcal/mol. The exothermicities of the  $CH_3$ -loss and  $C_2H_5$ -loss channels forming methyldiacetylene ( $CH_3CCCCH$ ) and diacetylene ( $HCCCCH$ ), respectively, are also shown.

Reactions of nonresonance-stabilized carbon-centered radicals with unsaturated hydrocarbons are expected to proceed via an intermediate<sup>16,17,69</sup> formed with almost no activation energy.<sup>45</sup> Subsequently, the short-lived intermediate decomposes to give the final products of the reaction whose isomeric structure depends upon the energy available in the system. Within the temperature range 74–295 K and pressure range 0.1–1 Torr, the measured total rate coefficient for the reaction is almost constant, and close to the collision-determined limit as mentioned above. This behavior suggests that back dissociation of the intermediate is negligible. Also for the reaction between  $C_2H$  and acetylene, as shown experimentally<sup>15,21,22</sup> and theoretically,<sup>15,70</sup> the entrance channel of the reaction is the attack of the  $\pi$  electrons by the radical to form an intermediate that in turn decomposes to give diacetylene as the final product, consistent

with an addition–elimination reaction. The hydrogen abstraction mechanism whereby a H-atom is captured by the  $C_2H$  radical to form acetylene is also thermodynamically feasible. In the case of  $C_2H + C_2H_2$ , Ceursters and co-workers<sup>15</sup> calculated a barrier of  $\sim 40\text{--}45$  kJ mol<sup>-1</sup> for the direct H-abstraction while addition–elimination of  $C_2H$  is essentially barrierless. The close to collision-determined limit rates of reaction indicate that addition–elimination predominates over abstraction in such reactions involving the  $C_2H$  radical with hydrocarbons.<sup>17</sup>

By analogy to the study of Ceursters and co-workers,<sup>15</sup> it is expected that the  $C_2H$  radical will add to the triple bond of the 1-butyne molecule. In principle, the  $C_2H$  addition proceeds by the direct attack on either of the triply bonded carbon atoms, giving rise to an acyclic radical species.<sup>15</sup> In the reaction of  $C_2H$  with acetylene, the cyclic three-membered and four-

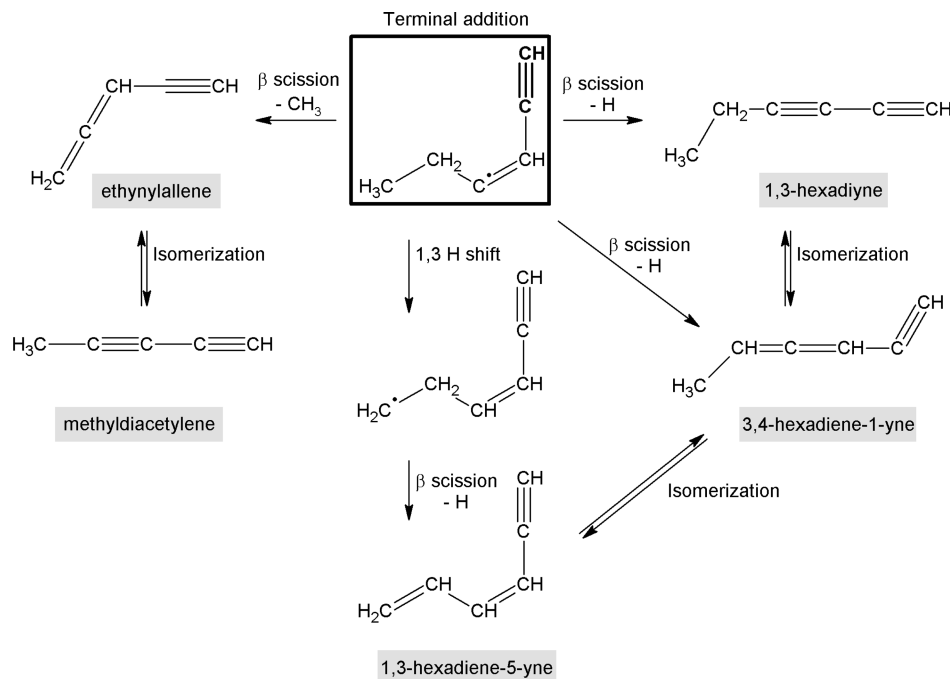


**Figure 10.** Proposed reaction pathways following addition of C<sub>2</sub>H radical (shown in bold characters) to the terminal acetylenic carbon atom in 1-butyne. The initial adduct formed is shown inside the rectangular frame.

membered ring radicals are found to be far less stable compared to the open radical structure. Moreover, the three-membered ring radical can easily rearrange to the open form because both structures are separated by a barrier of 5.7 kcal/mol (24 kJ/mol).<sup>15</sup> A similar situation can be expected for the title reaction. The initially formed radical can isomerize prior to dissociation. Senosiain and Miller<sup>71</sup> have reported several stationary points of C<sub>6</sub>H<sub>7</sub> related to the addition of acetylene to *n*- and *i*-C<sub>4</sub>H<sub>5</sub> radicals. The intermediates in those reactions are not directly relevant to the present reaction, but because the C<sub>2</sub>H + 1-butyne asymptote lies higher in energy than many of the calculated isomerization transition states, that work is consistent with relatively facile isomerization of the initially formed C<sub>6</sub>H<sub>7</sub> adduct in the C<sub>2</sub>H + 1-butyne reaction.

Starting with the radical formed by the direct attack of the terminal acetylenic carbon atom by C<sub>2</sub>H (see Figure 10), four different pathways leading to stable products (C<sub>5</sub>H<sub>4</sub> and C<sub>6</sub>H<sub>6</sub> isomers) can be proposed. These pathways include three different direct  $\beta$  scission reactions to ethynylallene formation via CH<sub>3</sub>-loss or either 1,3-hexadiyne or 3,4-hexadiene-1-yne via H-loss. A 1,3 H shift followed by a H-loss, through a  $\beta$  scission, could form another linear C<sub>6</sub>H<sub>6</sub> isomer, 1,3-hexadiene-5-yne. The barrier to a 1,3 H shift should be substantial,<sup>72</sup> but may still lie beneath the reactant energy.

Similarly, three different evolution pathways can be proposed in the case of C<sub>2</sub>H addition to the central carbon atom in the triple bond (see Figure 11). First, direct C<sub>2</sub>H<sub>5</sub>-loss through a  $\beta$  scission reaction can lead to diacetylene (C<sub>4</sub>H<sub>2</sub>). Second, a 1,4 H shift followed by  $\beta$  scission forms 2-ethynyl-1,3-butadiene or cyclization to a five-membered ring radical, which eventually decomposes to yield fulvene. Third, a 1,3 H shift followed by cyclization to form the four-membered radical structure can ultimately decompose to give 3,4-dimethylenecyclobut-1-ene through  $\beta$  scission.

On the basis of the proposed reaction pathways, the formation of C<sub>5</sub>H<sub>4</sub> isomers most probably results from terminal addition of the C<sub>2</sub>H radical to 1-butyne (see Figure 10). As seen from the PIE curve in Figure 7, the 4:1 ratio in favor of the

ethynylallene suggests that the diene is formed preferentially as opposed to methylidyneacetylene in the reaction between C<sub>2</sub>H with 1-butyne. This observation is consistent with the proposed mechanism where ethynylallene production is facile, because it results from a direct CH<sub>3</sub>-loss through a  $\beta$  scission reaction of the adduct formed after terminal addition. Ultimately, the branching ratio for isomerization to methylidyneacetylene will probably depend on the amount of internal energy left in ethynylallene after reaction. Moreover, the geometries of the adducts shown in Figure 10 and Figure 11 suggest that 1,4-pentadiyne formation is more complex than formation of ethynylallene. It can be argued that the rearrangement leading to its formation is probably unfavorable.

As suggested by the branching ratios of 18(±5)% and 32(±8)% for fulvene and 3,4-dimethylenecyclobut-1-ene (DMCB), respectively, four- and five-membered ring species are produced in comparable proportions to the linear C<sub>6</sub>H<sub>6</sub> isomers, i.e., 8(±5)% of 2-ethynyl-1,3-butadiene, 28(±8)% of 3,4-hexadiene-1-yne, and 14(±5)% of 1,3-hexadiene. At the present time, there is no potential energy surface available for the reaction between the C<sub>2</sub>H radical and C<sub>4</sub>H<sub>6</sub>. However, the related systems of *n*- and *i*-C<sub>4</sub>H<sub>5</sub> + acetylene<sup>71</sup> and the recombination of two propargyl radicals on a C<sub>6</sub>H<sub>6</sub> potential energy surface<sup>61</sup> provide some insight into possible isomerization pathways. The benzene molecule has the deepest well, on the C<sub>6</sub>H<sub>6</sub> surface, followed by fulvene and DMCB. Our measurements demonstrate that benzene is probably not formed in significant amounts by this reaction at room temperature, where an upper limit of 10% is estimated. The isomerization of DMCB or fulvene down to benzene must traverse substantial barriers. For instance, in the calculated fulvene to benzene paths,<sup>61</sup> benzene is the lower of the two isomers by about 31 kcal/mol (130 kJ/mol). However, approximately 75 kcal/mol (~314 kJ/mol) is required to overcome the barrier to isomerization. The presence of fulvene and DMCB products demonstrates that cyclization occurs in the C<sub>6</sub>H<sub>6</sub> + H channel but suggests that the energy remaining in the C<sub>6</sub>H<sub>6</sub> product is not enough to readily overcome the barrier to benzene formation. However,

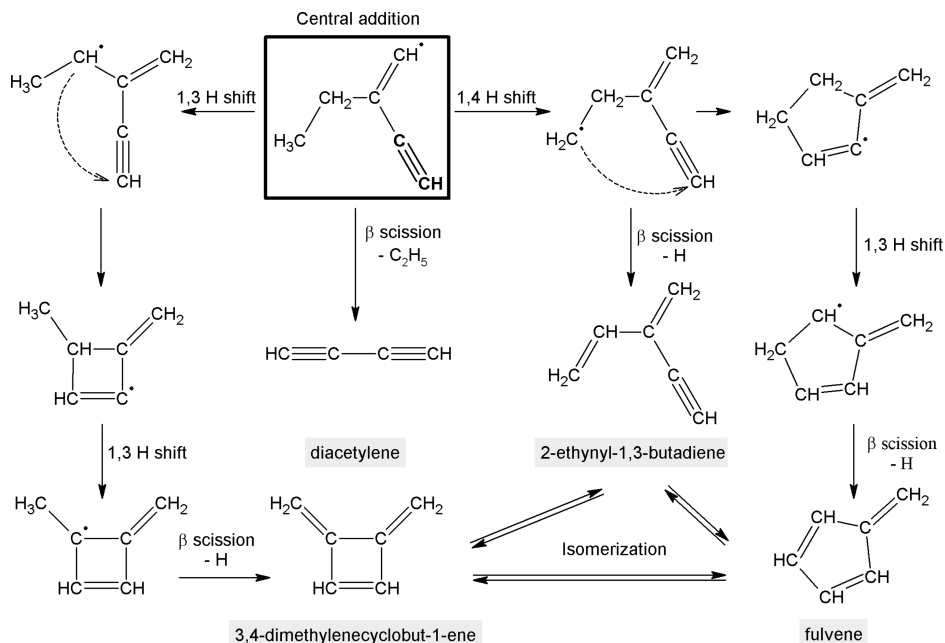


**Figure 11.** Proposed reaction pathways following addition of the C<sub>2</sub>H radical (shown in bold characters) to the central acetylenic carbon atom in 1-butyne. The initial adduct formed is shown inside the rectangular frame.

the isomerization on the C<sub>6</sub>H<sub>7</sub> surface may be more facile. Calculated transition states for the 1,5- and 1,3-H shifts from other C<sub>6</sub>H<sub>7</sub> isomers produced in the C<sub>4</sub>H<sub>5</sub> + acetylene reactions<sup>71</sup> lie near or below the energy of the C<sub>2</sub>H + 1-butyne reactants. It seems likely that the isomeric product distributions are largely determined by the dynamics on the C<sub>6</sub>H<sub>7</sub> surface. Although the total rate coefficient is found to be independent of temperature over the range studied, the product distributions could still be temperature dependent.

**4.2. Implication for Titan's Photochemistry.** Reactions of unsaturated C<sub>2</sub> hydrocarbon radicals<sup>73</sup> with hydrocarbon species are considered to play a central role for the formation of carbon-rich species (polyynes and PAHs) in the interstellar medium, exoplanets, and in the cold, photochemically active atmosphere on Titan.<sup>6,74</sup> In the course of these reactions, eventually two more carbon atoms are incorporated, thereby enlarging the carbon chain in the molecule and contributing to the complex process of molecular weight growth. These reactions can proceed via multiple intermediates, leading to different product channels and the initial isomeric structure can play a crucial role as demonstrated in the study with C<sub>3</sub>H<sub>4</sub> isomers.<sup>17</sup> Moreover, this study of 1-butyne shows that at least two competing product channels (H-loss and CH<sub>3</sub>-loss) are active and of almost equal importance. In the case of acetylene, the mechanism involves the initial addition of the C<sub>2</sub>H group to the π-electron system followed by the elimination of a hydrogen atom to form the product, diacetylene (C<sub>4</sub>H<sub>2</sub>). The measured rate constant is near the collision limit and increases as a function of the number of carbon atoms in the chain. In devising ever more elaborate models for Titan's atmosphere, low-temperature rate coefficient data including C<sub>4</sub> and longer chain hydrocarbons will be required. In this respect, the low-temperature kinetic measurements for the title reaction, together with the previous study of 1,3-butadiene<sup>39</sup> in our group, indicate that the reactions with C<sub>4</sub>H<sub>6</sub> isomers can occur at rates close to the collision limit at temperatures relevant to Titan's atmosphere, i.e., on the order of  $(2.5\text{--}3.0) \times 10^{-10} \text{ cm}^3 \text{ molecule}^{-1} \text{ s}^{-1}$ .

In this work, we also estimated the product branching ratios for the reaction of the C<sub>2</sub>H radical with 1-butyne at room

temperature and 4 Torr (533 Pa). Special care needs to be taken because it is known that extrapolation of data to lower temperatures is often problematic. However, the low-temperature kinetic measurements for the reaction of the ethynyl radical with 1-butyne do not show any temperature dependence in the range 74–295 K. This behavior is indicative of a reaction without an activation barrier. In this case, the rate-limiting step of the reaction is the addition of the C<sub>2</sub>H radical to the triple bond and the entrance channel of the reaction can be expected to be the same down to low temperatures as discussed by Goulay and co-workers.<sup>17</sup> It is therefore probable that reactions of the C<sub>2</sub>H radical with C<sub>4</sub>H<sub>6</sub> molecules can contribute to molecular weight growth through the addition and subsequent elimination of a H-atom or methyl radical giving rise to C<sub>5</sub> and C<sub>6</sub> carbonaceous species. Diacetylene could also be a favorable exit channel.

The distribution of C<sub>6</sub>H<sub>6</sub> isomers might be significantly altered at low temperatures. For instance, if thermal energy is required for isomerization of the initial adduct that leads to the formation of small four- and five-membered cyclic molecules, then this pathway could be disfavored at lower temperatures. However, the exothermicity of the reaction is substantial, and although Titan's atmosphere is cold, the low densities will limit collisional stabilization of intermediates; therefore most of the isomerization could still be enabled by chemical activation. Because of the numerous intermediates and transition states involved, with multiple product channels, further product detection studies of reactions involving the C<sub>2</sub>H radical with C<sub>4</sub>H<sub>6</sub> isomers, especially at low temperatures, are required to have a detailed cartography of these radical–molecule reactions.

## 5. Conclusion

Low-temperature rate coefficients (74–295 K) for the C<sub>2</sub>H + 1-butyne reaction are measured in a pulsed Laval nozzle apparatus. In this range, no apparent temperature dependence for the reaction is observed. This behavior is characteristic of a barrierless reaction at rates close to the collision limit, with the formation of an initial excited complex where the C<sub>2</sub>H radical

adds to the  $\text{—C}\equiv\text{C—}$  group of 1-butyne followed by elimination of either a hydrogen atom or methyl group. At room temperature, using MPIMS, two competing product channels have been identified:  $m/z = 64$  (C<sub>5</sub>H<sub>4</sub>) and  $m/z = 78$  (C<sub>6</sub>H<sub>6</sub>) consistent with the CH<sub>3</sub>- and H-loss channels for the reaction, respectively. Ethynylallene is identified as the main linear C<sub>5</sub>H<sub>4</sub> isomer and is formed in a 4:1 ratio to methyldiacetylene. This result is consistent with the proposed reaction pathways where ethynylallene is most likely formed through a direct  $\beta$ -scission after terminal addition. Interestingly, the C<sub>6</sub>H<sub>6</sub> product channel yields cyclic isomers, i.e., fulvene and 3,4-dimethylenecyclobut-1-ene, in almost equal proportions to linear isomers. However, the most stable C<sub>6</sub>H<sub>6</sub> isomer, benzene, is most probably not produced in this reaction. Diacetylene formation is also thermodynamically possible, but its presence or absence cannot be ascertained in our experiment. Our results suggest that in the cold, photochemically driven atmosphere of Titan, the formation of linear C<sub>6</sub>H<sub>6</sub> isomers should be favored at the expense of cyclic structures due to significant isomerization barriers down the potential energy surface to resonance stabilized structures. The measured rate constants and product branching ratios constitute key laboratory data for the development of chemical schemes in devising more elaborate models for planetary atmospheres, and in particular Titan. Further experimental and theoretical investigations involving the C<sub>2</sub>H radical with C<sub>4</sub> carbonaceous species are required to have a detailed cartography of the potential energy surfaces for these reactions.

**Acknowledgment.** The support of personnel (S.S.) for this research by the National Aeronautics and Space Administration (Grant No. NNX09AB60G) is gratefully acknowledged. We thank Mr. Howard Johnsen for excellent technical support. Sandia authors and instrumentation for this work are supported by the Division of Chemical Sciences, Geosciences and Biosciences, the Office of Basic Energy Sciences, the U.S. Department of Energy. Sandia is a multiprogram laboratory operated by Sandia Corporation, a Lockheed Martin Company, for the National Nuclear Security Administration under Contract No. DE-AC04-94-AL85000. The Advanced Light Source and Chemical Sciences Division (K.R.W. and S.R.L.) are supported by the Director, Office of Science, Office of Basic Energy Sciences of the U.S. Department of Energy under Contract No. DE-AC02-05CH11231 at the Lawrence Berkeley National Laboratory. A.J.T. acknowledges travel funding provided by the International Synchrotron Access Program (ISAP) managed by the Australian Synchrotron. The ISAP is funded by a National Collaborative Research Infrastructure Strategy grant provided by the Federal Government of Australia.

## References and Notes

- (1) Tucker, K. D.; Kutner, M. L.; Thaddeus, P. *Astrophys. J.* **1974**, *193*, L115.
- (2) Coustenis, A.; Bezaud, B. *Icarus* **1995**, *115*, 126.
- (3) Coustenis, A.; Bezaud, B.; Gautier, D. *Icarus* **1989**, *80*, 54.
- (4) Coustenis, A.; Bezaud, B.; Gautier, D.; Marten, A.; Samuelson, R. *Icarus* **1991**, *89*, 152.
- (5) Seki, K.; Okabe, H. *J. Phys. Chem.* **1993**, *97*, 5284.
- (6) Wilson, E. H.; Atreya, S. K. *Planet. Space Sci.* **2003**, *51*, 1017.
- (7) Sagan, C.; Khare, B. N.; Thompson, W. R.; McDonald, G. D.; Wing, M. R.; Bada, J. L.; Tuan, V. D.; Arakawa, E. T. *Astrophys. J.* **1993**, *414*, 399.
- (8) Cook, D. J.; Schlemmer, S.; Balucani, N.; Wagner, D. R.; Steiner, B.; Saykally, R. J. *Nature* **1996**, *380*, 227.
- (9) Snow, T. P.; Le Page, V.; Keheyian, Y.; Bierbaum, V. M. *Nature* **1998**, *391*, 259.
- (10) Coustenis, A.; Achterberg, R. K.; Conrath, B. J.; Jennings, D. E.; Marten, A.; Gautier, D.; Nixon, C. A.; Flasar, F. M.; Teanby, N. A.; Bezaud, B.; Samuelson, R. E.; Carlson, R. C.; Lellouch, E.; Bjoraker, G. L.; Romani, P. N.; Taylor, F. W.; Irwin, P. G. J.; Fouchet, T.; Hubert, A.; Orton, G. S.; Kunde, V. G.; Vinatier, S.; Mondellini, J.; Abbas, M. M.; Courtin, R. *Icarus* **2007**, *189*, 35.
- (11) Mebel, A. M.; Kislov, V. V.; Kaiser, R. I. *J. Am. Chem. Soc.* **2008**, *130*, 13618.
- (12) Wang, H.; Frenklach, M. *Combust. Flame* **1997**, *110*, 173.
- (13) Carty, D.; Le Page, V.; Sims, I. R.; Smith, I. W. M. *Chem. Phys. Lett.* **2001**, *344*, 310.
- (14) Ceursters, B.; Nguyen, H. M. T.; Peeters, J.; Nguyen, M. T. *Chem. Phys. Lett.* **2000**, *329*, 412.
- (15) Ceursters, P.; Nguyen, H. M. T.; Peeters, J.; Nguyen, M. T. *Chem. Phys.* **2000**, *262*, 243.
- (16) Goulay, F.; Leone, S. R. *J. Phys. Chem. A* **2006**, *110*, 1875.
- (17) Goulay, F.; Osborn, D. L.; Taatjes, C. A.; Zou, P.; Meloni, G.; Leone, S. R. *Phys. Chem. Chem. Phys.* **2007**, *9*, 4291.
- (18) Hoobler, R. J.; Leone, S. R. *J. Geophys. Res., [Planets]* **1997**, *102*, 28717.
- (19) Hoobler, R. J.; Leone, S. R. *J. Phys. Chem. A* **1999**, *103*, 1342.
- (20) Lander, A.; Mebel, A. M.; Kaiser, R. I. *Chem. Phys. Lett.* **2008**, *459*, 54.
- (21) Lee, S.; Hoobler, R. J.; Leone, S. R. *Rev. Sci. Instrum.* **2000**, *71*, 1816.
- (22) Lee, S.; Samuels, D. A.; Hoobler, R. J.; Leone, S. R. *J. Geophys. Res., [Planets]* **2000**, *105*, 15085.
- (23) Stahl, F.; Schleyer, P. V.; Bettinger, H. F.; Kaiser, R. I.; Lee, Y. T.; Schaefer, H. F. *J. Chem. Phys.* **2001**, *114*, 3476.
- (24) Vakhtin, A. B.; Heard, D. E.; Smith, I. W. M.; Leone, S. R. *Chem. Phys. Lett.* **2001**, *348*, 21.
- (25) Vakhtin, A. B.; Heard, D. E.; Smith, I. W. M.; Leone, S. R. *Chem. Phys. Lett.* **2001**, *344*, 317.
- (26) Zhang, F. T.; Kim, S.; Kaiser, R. I. *Phys. Chem. Chem. Phys.* **2009**, *11*, 4707.
- (27) Krasnopolsky, V. A. *Icarus* **2009**, *201*, 226.
- (28) Yung, Y. L.; Allen, M.; Pinto, J. P. *Astrophys. J., Suppl. Ser.* **1984**, *55*, 465.
- (29) Hebrard, E.; Dobrijevic, M.; Benilan, Y.; Raulin, F. *J. Photochem. Photobiol., C* **2006**, *7*, 211.
- (30) Hansmann, B.; Abel, B. *ChemPhysChem* **2007**, *8*, 343.
- (31) Dupeyrat, G.; Marquette, J. B.; Rowe, B. R. *Phys. Fluids* **1985**, *28*, 1273.
- (32) Rowe, B. R.; Dupeyrat, G.; Marquette, J. B.; Gauchere, P. *J. Chem. Phys.* **1984**, *80*, 4915.
- (33) Chastaing, D.; James, P. L.; Sims, I. R.; Smith, I. W. M. *Faraday Discuss.* **1998**, *109*, 165.
- (34) James, P. L.; Sims, I. R.; Smith, I. W. M.; Alexander, M. H.; Yang, M. B. *J. Chem. Phys.* **1998**, *109*, 3882.
- (35) Sims, I. R.; Smith, I. W. M. *Annu. Rev. Phys. Chem.* **1995**, *46*, 109.
- (36) Atkinson, D. B.; Jaramillo, V. I.; Smith, M. A. *J. Phys. Chem. A* **1997**, *101*, 3356.
- (37) Atkinson, D. B.; Smith, M. A. *J. Phys. Chem.* **1994**, *98*, 5797.
- (38) Berteloite, C.; Le Picard, S. D.; Birza, P.; Gazeau, M. C.; Canosa, A.; Benilan, Y.; Sims, I. R. *Icarus* **2008**, *194*, 746.
- (39) Nizamov, B.; Leone, S. R. *J. Phys. Chem. A* **2004**, *108*, 1746.
- (40) Vuitton, V.; Doussin, J. F.; Benilan, Y.; Raulin, F.; Gazeau, M. C. *Icarus* **2006**, *185*, 287.
- (41) Vuitton, V.; Yelle, R. V.; Cui, J. J. *Geophys. Res., [Planets]* **2008**, *113*, 18.
- (42) Lavvas, P. P.; Coustenis, A.; Vardavas, I. M. *Planet. Space Sci.* **2008**, *56*, 27.
- (43) Lavvas, P. P.; Coustenis, A.; Vardavas, I. M. *Planet. Space Sci.* **2008**, *56*, 67.
- (44) Hansen, N.; Miller, J. A.; Kasper, T.; Kohse-Hoinghaus, K.; Westmoreland, P. R.; Wang, J.; Cool, T. A. *Proc. Combust. Inst.* **2009**, *32*, 623.
- (45) Vanlook, H.; Peeters, J. *J. Phys. Chem.* **1995**, *99*, 16284.
- (46) Montgomery, J. A.; Frisch, M. J.; Ochterski, J. W.; Petersson, G. A. *J. Chem. Phys.* **1999**, *110*, 2822.
- (47) Montgomery, J. A.; Frisch, M. J.; Ochterski, J. W.; Petersson, G. A. *J. Chem. Phys.* **2000**, *112*, 6532.
- (48) Ervin, K. M., *PESCAL, Fortran program*, 2009.
- (49) Ervin, K. M.; Ramond, T. M.; Davico, G. E.; Schwartz, R. L.; Casey, S. M.; Lineberger, W. C. *J. Phys. Chem. A* **2001**, *105*, 10822.
- (50) Osborn, D. L.; Zou, P.; Johnsen, H.; Hayden, C. C.; Taatjes, C. A.; Knyazev, V. D.; North, S. W.; Peterka, D. S.; Ahmed, M.; Leone, S. R. *Rev. Sci. Instrum.* **2008**, *79*.
- (51) Slagle, I. R.; Yamada, F.; Gutman, D. *J. Am. Chem. Soc.* **1981**, *103*, 149.
- (52) Meloni, G.; Selby, T. M.; Goulay, F.; Leone, S. R.; Osborn, D. L.; Taatjes, C. A. *J. Am. Chem. Soc.* **2007**, *129*, 14019.
- (53) Minsek, D. W.; Chen, P. *J. Phys. Chem.* **1990**, *94*, 8399.
- (54) Bieri, G.; Burger, F.; Heilbronner, E.; Maier, J. P. *Helv. Chim. Acta* **1977**, *60*, 2213.



- (55) Kiess, N. H.; Broida, H. P. *Astrophys. J.* **1956**, *123*, 166.
- (56) Cvejanovic, D.; Adams, A.; King, G. C. *J. Phys. B: At., Mol. Opt. Phys.* **1978**, *11*, 1653.
- (57) Sander, R. K.; Tjee, J. J.; Quick, C. R.; Romero, R. J. *J. Chem. Phys.* **1988**, *89*, 3495.
- (58) Nakayama, T.; Watanabe, K. *J. Chem. Phys.* **1964**, *40*, 558.
- (59) Laufer, A. H.; Fahr, A. *Chem. Rev.* **2004**, *104*, 2813.
- (60) Berkowitz, J.; Ellison, G. B.; Gutman, D. *J. Phys. Chem.* **1994**, *98*, 2744.
- (61) Miller, J. A.; Klippenstein, S. J. *J. Phys. Chem. A* **2003**, *107*, 7783.
- (62) Hansen, N.; Klippenstein, S. J.; Miller, J. A.; Wang, J.; Cool, T. A.; Law, M. E.; Westmoreland, P. R.; Kasper, T.; Kohse-Hoinghaus, K. *J. Phys. Chem. A* **2006**, *110*, 4376.
- (63) Bobeldijk, M.; Vanderzande, W. J.; Kistemaker, P. G. *Chem. Phys.* **1994**, *179*, 125.
- (64) Fahr, A.; Selby, T. M.; Osborn, D. L.; Taatjes, C. A. Private communication, 2006.
- (65) Nemeth, G. I.; Selzle, H. L.; Schlag, E. W. *Chem. Phys. Lett.* **1993**, *215*, 151.
- (66) Rosenstock, H. M.; Dannacher, J.; Liebman, J. F. *Radiat. Phys. Chem.* **1982**, *20*, 7.
- (67) Masclet, P.; Mouvier, G.; Bocquet, J. F. *J. Chim. Phys. Phys.-Chim. Biol.* **1981**, *78*, 99.
- (68) Beez, M.; Bieri, G.; Bock, H.; Heilbron, E. *Helv. Chim. Acta* **1973**, *56*, 1028.
- (69) Goulay, F.; Rebrion-Rowe, C.; Biennier, L.; Le Picard, S. D.; Canosa, A.; Rowe, B. R. *J. Phys. Chem. A* **2006**, *110*, 3132.
- (70) Herbst, E.; Woon, D. E. *Astrophys. J.* **1997**, *489*, 109.
- (71) Senosiain, J. P.; Miller, J. A. *J. Phys. Chem. A* **2007**, *111*, 3740.
- (72) Matheu, D. M.; Green, W. H.; Grenda, J. M. *Int. J. Chem. Kinet.* **2003**, *35*, 95.
- (73) Laufer, A. H.; Fahr, A. *Chem. Rev.* **2004**, *104*, 2813.
- (74) Woon, D. E.; Park, J. Y. *Icarus* **2009**, *202*, 642.
- (75) Maier, J. P. *Angew Chem., Int. Ed. Engl.* **1981**, *20*, 638.
- (76) Hayaishi, T.; Iwata, S.; Sasanuma, M.; Ishiguro, E.; Morioka, Y.; Iida, Y.; Nakamura, M. *J. Phys. B: At., Mol. Opt. Phys.* **1982**, *15*, 79.

JP911132R